SECTION A

CHAPTER 2

Introduction

2.1 Electrochemistry: An Overview

2.1.1. *Basic concepts*

Electrochemistry, as the name suggests, studies the relationship between electrical and chemical occurrences.[1] It covers mainly two areas: *electrolysis*-conversion of chemical compounds by passage of an electric current and *electrochemical power sources*-energy of chemical reactions transformed into electricity. Electrochemistry is one effective technique to study electron transfer properties. When electron transfer is between a solid substrate and a solution species, it is termed heterogeneous process. Inversely, if electron transfer reaction occurs between two species, both of which are in solution, the reaction is homogeneous. Therefore, electrochemistry can specifically be defined as the science of structures and processes at and through the interface between an electronic (electrode) and an ionic conductor (electrolyte) or between two ionic conductors.[2]

Electrochemistry is an interdisciplinary science that is mainly rooted in chemistry and physics; however, also linked to engineering and biochemistry/biology. Due to its diversity, electrochemistry has found application in various working fields such as: analytical electrochemistry; environmental electrochemistry;[3] electrochemistry of glasses;[4] ionic liquids electrochemistry; microelectrochemistry,

nanoelectrochemistry; photoelectrochemistry;[3] solid state electrochemistry; solution electrochemistry; surface electrochemistry; technical electrochemistry with numerous subtopics such as: Batteries and energy storage[5]; Corrosion and corrosion inhibition; Electrochemical synthesis and reactors (electrosynthesis); Electronic components (capacitors, displays, information storage, rectifiers); Fuel cells and galvanic deposition; Theoretical or quantum electrochemistry.

Electrochemistry also involves the measurement of potential (potentiometry) or current response (voltammetry).[6] The work described in this dissertation involves current measurement, voltammetry and a number of voltammetric techniques, namely, cyclic voltammetry (CV), linear sweep voltammetry (LSV), square wave voltammetry (SWV), chronoamperometry (CA) and chronocoulometry.

2.1.1.1. *The electrode-solution interface*

The interface between a metal (electrode) and an electrolyte solution is considered when trying to gain an impression of the structures and processes that occur in electrochemical systems. Figure 2.1 shows a schematic diagram of the interface structure and the processes. This interface is generally charged; the metal surface carries an excess charge, which is balanced by a charge of equal magnitude and opposite sign on the solution side of the interface. The resulting charge distribution; two narrow regions of equal and opposite

charge, is known as the electric double layer. It can be viewed as a capacitor with an extremely small effective plate separation, and therefore has a very high capacitance.

Reactions involving charge transfer through the interface, and hence the flow of a current, are called electrochemical reactions. Two types of such reactions can occur at the interface. One is an instance of metal deposition. It involves the transfer of a metal ion from the solution onto the metal surface, where it is discharged by taking up electrons. Metal deposition takes place at specific sites. The deposited metal ion may belong to the same species as those on the metal electrode, as in the deposition of a Ag^+ ion on a silver electrode, or it can be different as in the deposition of a Ag^+ ion on platinum. In any case the reaction is formally written as:

$$Ag^+(solution) + e^- (metal) \rightleftharpoons Ag(metal) \qquad (2.1)$$

Metal deposition is an example of a more general class of electrochemical reactions, ion transfer reactions. In these an ion, e.g. a proton or a halide ion, is transferred from the solution to the electrode surface, where it is subsequently discharged.

Another type of electrochemical reaction, is an electron-transfer reaction, an oxidized species is reduced by taking up an electron from the metal. Since electrons are very light particles, they can tunnel over a distance of 10 Å or more, and the reacting species need not be in contact with the metal surface. The oxidized and the reduced forms of

the reactants can be either ions or uncharged species. A typical example for an electron-transfer reaction is:

$$Fe^{3+}(solution) + e^{-}(metal) \rightleftharpoons Fe^{2+}(metal) \qquad (2.2)$$

Both ion and electron transfer reactions entail the transfer of charge through the interface, which can be measured as the electric current. Based on the definition of the electric double layer, Helmholtz[7] proposed a simple geometric model of the interface. This model gave rise to the concept of the inner and outer Helmholtz planes (layers). The *inner Helmholtz layer* comprises all species that are specifically adsorbed on the electrode surface. If only one type of molecule or ion is adsorbed, and they all sit in equivalent positions, then their centres define the *inner Helmholtz plane* (IHP). The *outer Helmholtz layer* comprises the ions that are closest to the electrode surface, but are not specifically adsorbed. They have kept their solvation spheres intact, and are bound only by electrostatic forces. If all these ions are equivalent, their centres define the *outer Helmholtz plane* (OHP). The layer which extends from the OHP into the bulk solution is a three dimensional region of scattered ions called the diffuse or Gouy layer. The IHP and OHP represent the layer of charges which is strongly held by the electrode and can survive even when the electrode is pulled out of the solution.[8,9]

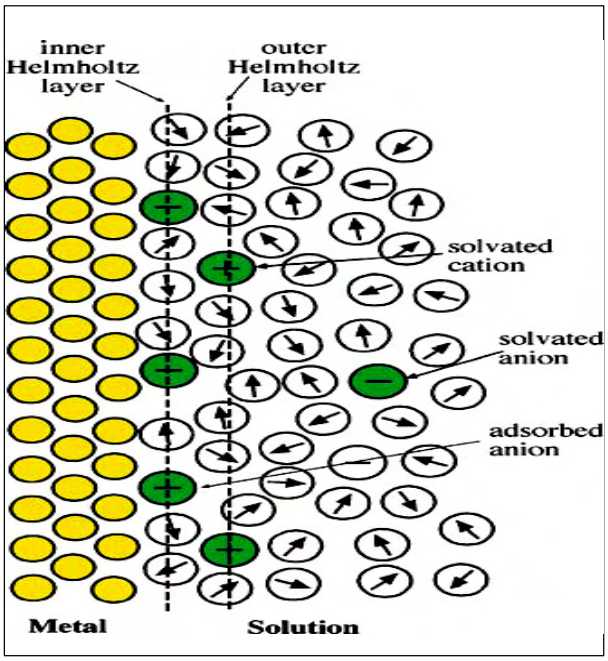

Figure 2.1: *Model of the electrode-solution double layer*[2]

2.1.1.2. *Faradaic and non-Faradaic processes*

Faraday's law states that *the number of moles of a substance, produced or consumed during an electrode process, is proportional to the electric charge passed through the electrode*; Redox processes are often governed by this law. Electron transfer reactions proceeding at the charged interface obeying this law are called Faradaic process. Non-Faradaic process arise when an electrode-solution interface shows a range of potentials where no charge-transfer reactions occur. However, processes such as adsorption and desorption can occur, and the structure of the electrode-solution interface can change with changing potential or solution composition. Although charge does not

cross the interface, external currents can flow (at least transiently) when the potential, electrode area, or solution composition changes.

2.1.1.3. *Mass transport processes*

The movement of charged or neutral species that allows the flow of electricity through an electrolyte solution in an electrochemical cell is referred to as a mass transport process. **Migration**, **diffusion** and **convection** are the three possible mass transport processes accompanying an electrode reaction.

Migration: Migration is the movement of charged particles along an electrical field; this charge is carried through the solution by ions. To limit migrational transport of the ions that are components of the redox system examined in the cell, excess supporting electrolyte is added to the solution; in this work a large concentration of KCl is used. In analytical applications, the presence of a high concentration of supporting electrolyte which is hundred times higher than the concentration of electroactive ions means that the contribution of examined ions to the migrational transport is less than one percent. Then it can be assumed that the transport of the examined species towards the working electrode is by diffusion only. Migration of electroactive species can either enhance or diminish the current flowing at the electrode during reduction or oxidation of cations. It helps reduce the electrical field by increasing the solution conductivity, and

serves to decrease or eliminate sample matrix effects. The supporting electrolyte ensures that the double layer remains thin with respect to the diffusion layer, and it establishes a uniform ionic strength throughout the solution. However, measuring the current under mixed migration-diffusion conditions may be advantageous in particular electrochemical and electroanalytical situations.[1] Uncharged molecules do not migrate.

Diffusion: Diffusion is the transport of particles as a result of local difference in the chemical potential.[10] Diffusion is simply the movement of material from a high concentration region of the solution to a low concentration region. Electrochemical reactions are heterogeneous and hence they are frequently controlled by diffusion. If the potential at an electrode oxidizes or reduces the analyte, its concentration at the electrode surface will be lowered, and therefore, more analyte moves to the electrode from the bulk of the solution, which makes it the main current-limiting factor in voltammetric process. Although migration carries the current in the bulk solution during electrolysis, diffusion should also be considered because, as the reagent is consumed or the product is formed at the electrode, concentration gradient between the vicinity of the electrodes and the electroactive species arise. Indeed, under some circumstances, the flux of electroactive species to the electrode is due almost completely to diffusion.

Convection: Convection is one of the modes of mass transport which involves the movement of the whole solution carrying the charged

particles. The major driving force for convection is an external mechanical energy associated with stirring or flow of the solution or rotating or vibrating the electrode (forced convection). Convection can also occur naturally as a result of density gradient.[11] In voltammetry, convection is eliminated by maintaining the cell under quiet and stable condition.

2.1.2. *Voltammetry*

Voltammetry is the measurement of current as a function of a controlled electrode potential and time. The resultant current–voltage (or current–time or current–voltage–time) display is commonly referred to as the "voltammogram".[1,12] The term "voltammetry" was coined by Laitinen and Kolthoff.[13,14] The objectives of a voltammetric experiment also vary, ranging from analytical measurements designed to determine the concentration of an analyte to measurements designed to elucidate complex mechanisms and the values of the associated thermodynamic and kinetic parameters.[1] The protocol for potential control may vary, leading to a number of different techniques each with their common names. The techniques used in this work are cyclic voltammetry (CV), linear sweep voltammetry (LSV), square wave voltammetry (SWV), chronoamperometry (CA) and chronocoulometry. This section gives the basic theoretical background underlying these techniques.

2.1.2.1. *Cyclic voltammetry*

This is a commonly employed type of voltammetry where measurement of the current response of an electrode to a linearly increasing and decreasing potential cycle is performed.[15] Figure 2.2 presents the resulting scan of potential against time, scanning linearly the potential of a stationary working electrode in an unstirred solution, using a triangular potential waveform and the corresponding voltammogram. The experiment is usually started at a potential where no electrode process occurs (0.2 V in the plot) and the potential is scanned with a fixed scan rate to the switching potential (0.7 V in the plot). When an electrochemically active compound is present in the solution phase, an anodic current peak at the potential E_{pa} is detected with the peak current I_{pa}. When the potential is swept back during the reverse scan a further current peak at the potential E_{pc} may be observed with a cathodic peak current I_{pc}.

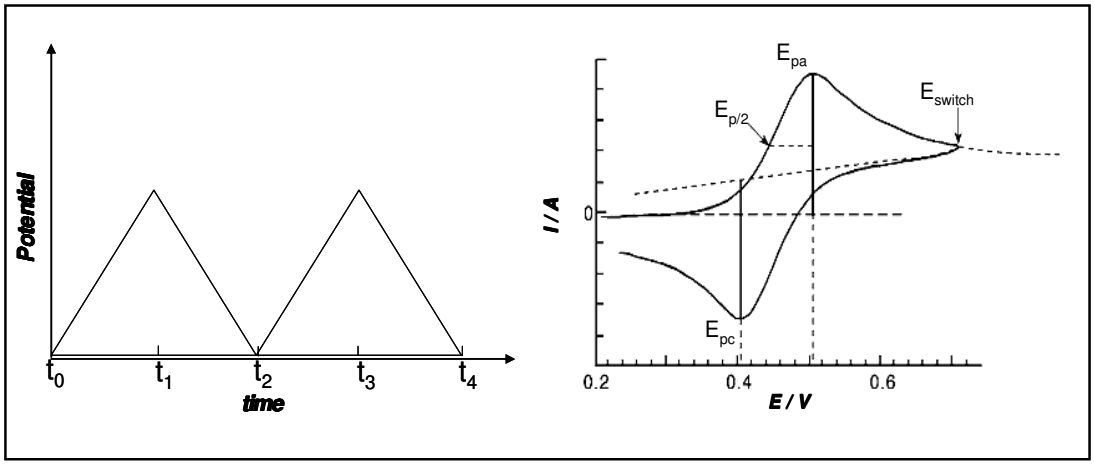

Figure 2.2: *The potential-time waveform and a typical cyclic voltammogram for a reversible redox process*

Cyclic voltammetry is an excellent technique to survey the reactivity of new materials or compounds and can provide information about (i) the potential at which oxidation or reduction processes occur, (ii) the oxidation state of the redox species, (iii) the number of electrons involved, (iv) the rate of electron transfer, (v) possible chemical processes associated with the electron transfer, and (vi) adsorption effects,[1,16,17] etc. Electron transfer processes can be labelled reversible, irreversible or quasi-reversible, and are identified by certain criteria that can be measured by cyclic voltammetry.

1.1.2.1.1. *Reversibility*

Electrochemical reversibility is a practical concept used when the surface concentrations of both species of a redox couple obey the Nernst equation (equation 2.3) at any potential difference applied at the electrode-solution interface. In short, it means that the Nernst equation can be applied also when the actual electrode potential (E) is higher (anodic reaction) or lower (cathodic reaction) than the equilibrium potential (E_e). Therefore, such a process is called a reversible or Nernstian reaction.

$$E = E^\circ + \frac{RT}{nF}\ln\frac{c_O(x=0)}{c_R(x=0)} \approx E^\circ + \frac{2.303RT}{nF}\log\frac{c_O(x=0)}{c_R(x=0)} \qquad (2.3)$$

where $c_O(x=0)$ and $c_R(x=0)$ are the concentrations of these species at the electrode surface, E° is the formal electrode potential, n is the

number of electrons transferred, F is Faraday's constant, RT have their usual meaning. It follows that the Nernst equation expresses the relationship between the surface concentrations and the electrode potential regardless of the current flow. It should also be mentioned that the appearance of the reversible behaviour depends on the relative value of electron transfer rate (k_s) and mass transport, since no equilibrium exists between the surface and bulk concentrations, reactants are continuously transported to the electrode surface by diffusion.

The magnitude of the peak current for a reversible electron transfer is given by the *Randles–Ševčik* equation (2.4)[1]

$$I_p = 0.446nFAc\sqrt{\frac{nF\nu D}{RT}} \approx (2.69\,x10^5)n^{3/2}AD^{1/2}c\nu^{1/2} \qquad (2.4)$$

In this equation the peak current I_p is dependent on n, the number of electrons transferred per molecule diffusing to the electrode surface, F, the Faraday constant, A, the electrode area, c, the concentration of analyte in solution, R, the gas constant, T, the absolute temperature, ν, the scan rate, and D, the diffusion coefficient.

The dependence of current on the scan rate is indicative of electrode reaction controlled by diffusion,[18,19,20] using equation (2.4) a linear plot of I_p vs. $\nu^{1/2}$ is obtained. Deviation from linearity indicates the presence of chemical reaction involving either the oxidized, reduced or both species.

For a reversible process, the half-wave potential, $E_{½}$, is related to the standard potential ($E°$) as in equation (2.5):

$$E_{½} = E^{\circ} + \frac{RT}{2nF} \ln \frac{[O]}{[R]} \qquad (2.5)$$

where R is the gas constant, T the temperature in Kelvin, F the Faraday constant and [O] is the concentration of oxidised species, [R] is the concentration of reduced species in mol L^{-1}. The half-wave potential, $E_{1/2}$ can be calculated from equation (2.6):

$$E_{½} = \frac{E_{pa} + E_{pc}}{2} \qquad (2.6)$$

where E_{pa} is the anodic peak potential and E_{pc} is the cathodic peak potential. The number of electrons transferred in a reversible process can be calculated from equation (2.8):

$$\Delta E = E_{pc} - E_{pa} = \frac{RT}{nF} \quad , \quad \text{at } 25^{0}\text{C} \qquad (2.7)$$

$$\Delta E = \frac{0.059\ V}{n} \qquad (2.8)$$

where n is the number of electrons transferred, other symbols have their usual meaning. The peak-to-peak separation is approximately 59 mV at 298 K and is independent of scan rate.

1.1.2.1.2. *Irreversibility*

Irreversibility in electrochemistry is when the charge-transfer step is very sluggish, i.e., the standard rate constant (k_s) and exchange current density (j_o) are very small.[7] In this case the anodic and cathodic reactions are never simultaneously significant. In order to observe any current, the charge-transfer reaction has to be strongly activated either in cathodic or in anodic direction by application of overpotential. These processes are characterized by a shift of the peak potential with the scan rate and ΔE can be calculated from equation (2.9).[1,21]

$$\Delta E = E^o - \frac{RT}{\alpha n_a F}\left[0.78 - \ln\frac{k^o}{D^{1/2}} + \ln\left(\frac{\alpha n_a F}{RT}\nu\right)^{1/2}\right] \qquad (2.9)$$

where α is the electron transfer coefficient of the rate determing step and n_α is the number of electrons involved in the charge transfer step and k^o is the standard electrode reaction rate constant in cms^{-1}. The other symbols are listed in the list of symbols. At 25°C, the peak potential and the half-peak potential differ by $0.048\ V/\alpha n$. Hence, the voltammogram becomes more drawn-out as αn decreases. In an irreversible process, only forward oxidation or reverse reduction peak is observed, see Figure 2.3. It is common to observe a weak reverse peak at increased scan rates during forward oxidation at times, because of sluggish electron exchange as mentioned above. The Nernst equation is not applicable in the case of irreversible process. This is

due to the rate of electron transfer insufficient to maintain surface equilibrium and thus the oxidized and reduced species are not at equilibrium**.**

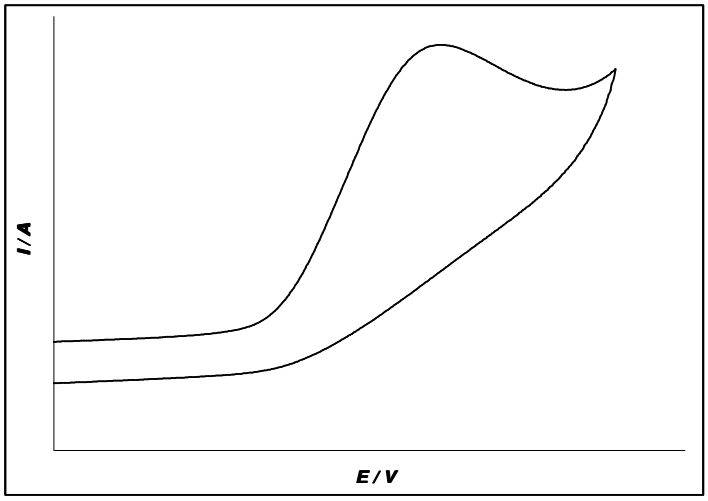

Figure 2.3*: Typical cyclic voltammogram for an irreversible redox process*

The peak current, I_p for an irreversible process can be calculated from equation (2.10):

$$I_p = \left(2.99x10^5\right)n[(1-\alpha)n]^{1/2} AcD^{1/2}\nu^{1/2} \qquad (2.10)$$

where α denotes the electron transfer coefficient and n the number electrons transferred in the rate determining step.

1.1.2.1.3. *Quasi-reversibility*

Mass transport plays a major role in controlling the concentration of the redox couple and the expressions for reversible processes also apply for quasi-reversible processes. The voltammograms of a quasi-reversible process exhibit a large peak-to-peak separation compared to reversible processes. The peak current increase with $\nu^{1/2}$ but is not

linear and Δ*E* is greater than 0.059/n V. In reversible process, current is controlled purely by mass transport but in quasi-reversible process, current is controlled by both the mass transport and charge transfer kinetics.[22,23]

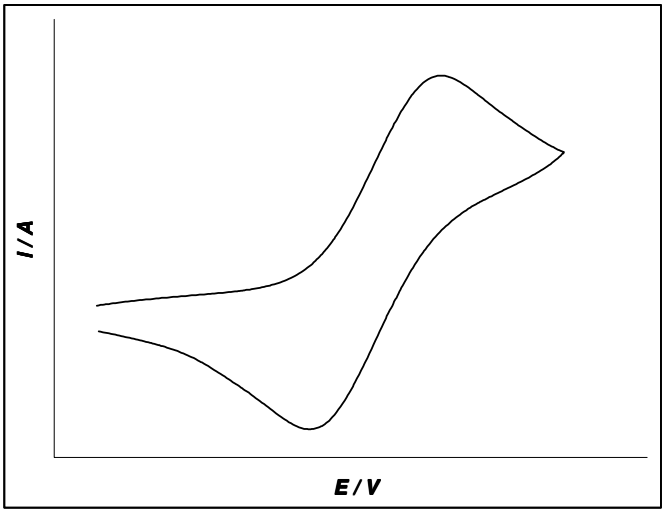

***Figure 2.4**: Typical cyclic voltammogram for a quasi-reversible redox process*

When cyclic voltammetry is applied to immobilised redox systems such as self-assembled monolayer (SAM) at an electrode surface, distinct peak shape and peak currents as depicted in Figure 2.5 may be observed. The peak current now becomes directly proportional to the scan rate.

$$I_p = \frac{n^2 F^2 \Gamma A \nu}{4RT} \qquad (2.11)$$

In this equation the peak current I_p is directly proportional to ν, the scan rate, and Γ the surface concentration for the immobilised redox system. A plot of $\log I_p$ vs. $\log \nu$ allows diffusion controlled processes and

processes involving surface immobilised redox systems to be distinguished. When the slope of the plot is 0.5 or 1 it is a diffusion controlled process, or a surface confined (adsorption) process, respectively. The slight differences in cyclic voltammetric processes is summarised in Table 2.1.

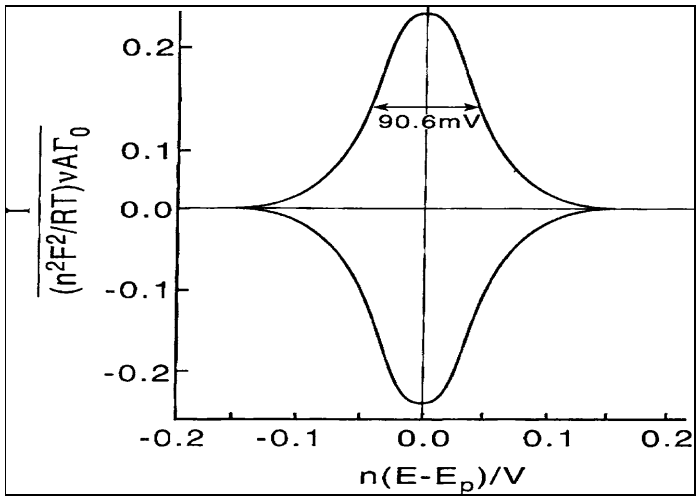

Figure 2.5: Symmetric "bell-shaped" cyclic voltammogram for surface confined redox system[7]

Table 2.1: *The diagnostic criteria for reversible, irreversible and quasi-reversible cyclic voltammetric process*

Parameter	**Cyclic Voltammetry Process**		
	Reversible	Irreversible	Quasi-reversible
E_p	Independent of ν	Shifts cathodically by $30/\alpha n$ mV for 10-fold increase in V	Shifts with ν
$\Delta E_p = E_{pa} - E_{pc}$	~ 59/n mV at 25°C and independent of ν	-	May approach 60/n mV at low ν but increases as ν increases
$I_p / \nu^{1/2}$	Constant	Constant	Virtually independent of ν
I_{pa} / i_{pc}	Equals 1 and independent of ν	For a reduction process, < 1	Equals 1 only for α=0.5

2.1.2.2. *Linear sweep voltammetry*

Linear sweep voltammetry (LSV) is a method where there is linear variation of the electrode potential with time with the scan rate (ν), ν = dE/dt and current versus potential is recorded. In LSV essentially only the first half-cycle of a cyclic voltammogram is executed. Scanning starts at a potential where no electrochemical reaction occurs. Current can be observed at the potential where the charge transfer begins, which increases with the potential, however, after a maximum value (peak current plateau) it starts to decrease due to the depletion of the reacting species at the interface.

LSV is employed in the rotating disk electrochemistry (RDE). A rotating disk electrode is rotated in the solution under study and the current depends on the solution flow rate. For the rotating disk electrode, the time dependence is in the rotation rate of the disk, which in turn controls the solution velocity near the electrode. The rate of mass transport at the rotating disk electrode is varied by altering the disk rotation speed[24]. The rotating electrode is mounted vertically to a controllable-speed motor and rotated with constant angular velocity. The components of the fluid velocity depends on this angular velocity of the disk, which is given by $\omega = 2\pi f$, where f is the rotation speed in revolutions per minutes (rpm) or rotation frequency in hertz. It depends on other factors such as the radial distance from the centre of the disk (r), the coefficient of kinematic viscosity of the fluid (γ) and on the axial distance from the surface of the disk.[25]

A general equation of the disk current, taking into account both mass transport and electron transfer kinetics can thus be given as the Koutečky-Levich equation[26]:

$$\frac{1}{j} = \frac{1}{j_k} + \frac{1}{j_{\lim}} \qquad (2.12)$$

where j is the measured current density, j_k the disk current density in the absence of diffusion control, for electron transfer controlled process is given by

$$j_k = Fk(E)c \qquad (2.13)$$

with the catalytic rate constant k as a function of the electrode potential E and the concentration c. The diffusion-limited current $j_{\lim}$ at the rotating disk electrode is given by the Levich equation[7] based totally on mass-transfer limited conditions.

$$j_{\lim} = 0.21nFcD^{\frac{2}{3}}\omega^{\frac{1}{2}}\gamma^{\frac{1}{6}} \qquad (2.14)$$

where, n is the number of electrons transferred per molecule, F is the Faraday constant, D is the diffusion coefficient, ω is the rotation rate in rpm, and γ is the kinematic viscosity of the solution.

2.1.2.3. *Square wave voltammetry*

Square-wave voltammetry is a large-amplitude differential technique in which a wave form composed of a symmetric square wave, superimposed on a base staircase potential, is applied to the working electrode (Figure 2.6).[27] The current is sampled twice during

each square wave cycle, once at the end of the forward pulse and once at the end of the reverse pulse. The current at the end of the forward pulse, I_f, and the current at the end of the reverse pulse I_b, are both registered as a function of staircase potential, which is midway between the potentials corresponding to the forward and backward potential steps. The difference between the two measurements is plotted versus the base staircase potential. Since I_f and I_b usually have opposite signs, the difference is larger than each individual component in the region of the peak that is centred on the half-wave potential.

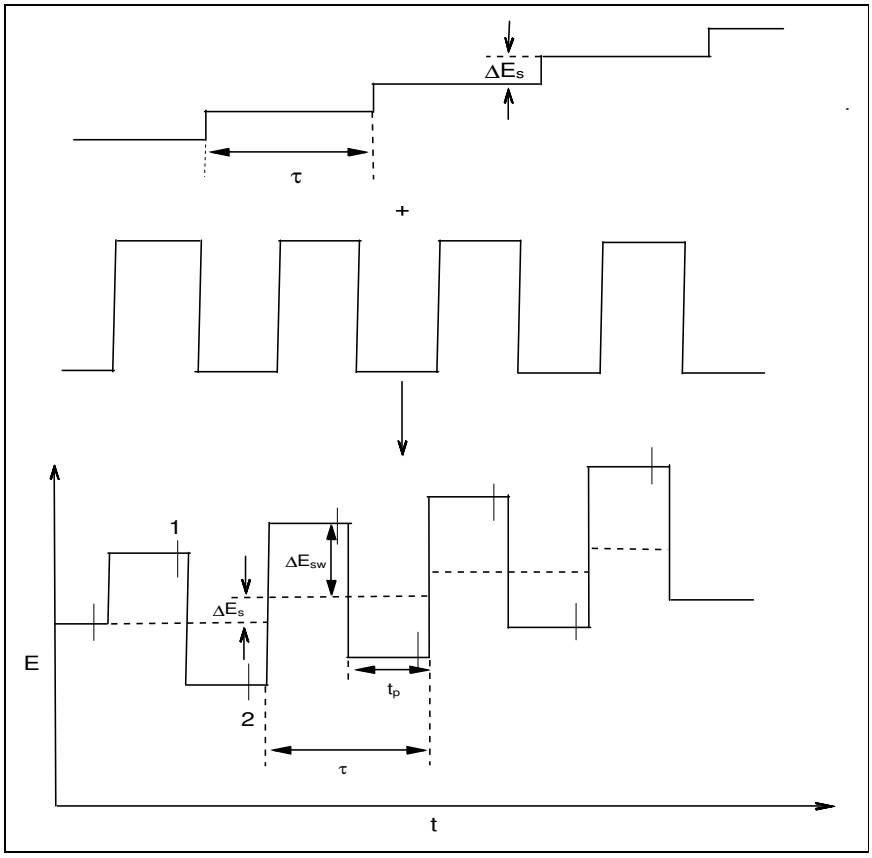

***Figure 2.6**: Square wave voltammetry potential-time waveform: sum of staircase and synchronized square wave*

Square-wave voltammetry is characterised by four parameters: square wave period, τ, pulse width, $t_p = \tau/2$, step height, ΔE_s and pulse height, ΔE_{sw}. The pulse width is related to the square wave frequency, $f = 1/(2t_p)$ and as the staircase step at the beginning of each cycle is ΔE_s, it means that the effective scan rate is $\nu = \Delta E_s/2t_p = f\,\Delta E_s$. The major advantage of square-wave voltammetry is its speed and excellent sensitivity.[28,29] A complete voltammogram can be recorded within a few seconds. The peak height is directly proportional to the concentration of the electroactive species and direct detection limit as low as 10^{-8} mol.L^{-1} is possible. This technique includes the use of faster scan rates compared to conventional differential pulse voltammetry. Applications of square-wave voltammetry include the study of electrode kinetics with regard to catalytic homogeneous chemical reactions, and determination of some species at trace levels. In this research, a computer-controlled square wave voltammetry was employed. Figure 2.7 displays a typical square-wave voltammogram.

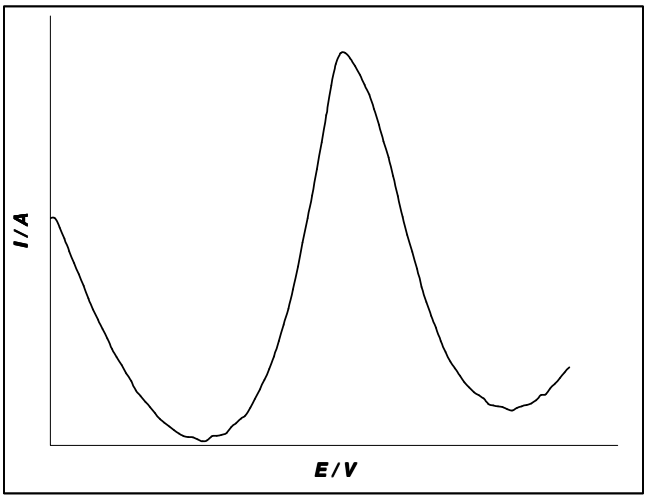

***Figure 2.7**: Typical square wave voltammetric response*

2.1.2.4. *Chronoamperometry*

When the potential of a working electrode is stepped from a value at which no Faradaic reaction occurs to a potential at which the surface concentration is effectively zero, is referred to as chronoamperometry. In chronoamperometry the current is measured as a function of time after application of a potential step perturbation. For example, in Figure 2.8a, if the potential is stepped from E_1, where no current flows, i.e., where the oxidation or reduction of the electrochemically active species does not take place, to E_2 where the current belongs to the electrode reaction. The electrode reaction is diffusion limited. The resulting current-time dependence is monitored. The current-time curve reflects the change in the concentration gradient in the vicinity of the surface. This involves a gradual expansion of the diffusion layer associated with the depletion of the reactant as time progresses, consequently the current decays with time (at a planar electrode) (Figure 2.8b). The current flows at any time after application of the potential step will obey the Cottrell equation.[1]

$$i(t) = \frac{nFAcD^{1/2}}{\pi^{1/2}t^{1/2}} = kt^{-1/2} \qquad (2.15)$$

where n, F, A, c, D, and t are the number of electrons, Faradayconstant, the surface area, the concentration, the diffusion coefficient, and time respectively.

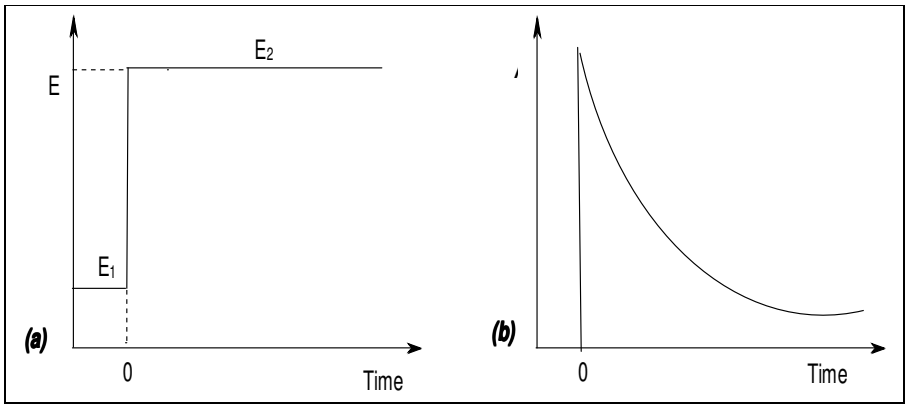

***Figure 2.8**: Potential step chronoamperometry: (a) schematic application of potential step and (b) chronoamperometric response*

Chronoamperometry is often used for measuring the diffusion coefficient of electroactive species or the surface area of the working electrode. It can also be applied to the study of mechanisms of electrode processes.[30,31]

2.1.2.5. *Chronocoulometry*

Chronocoulometry belongs to a family of step techniques[31,32] just like chronoamperometry. However, unlike chronoamperometry where current-time dependence is monitored, the charge-time dependence is measured in chronocoulometry. Chronocoulometry gives practically the same information that is provided by chronoamperometry, since it is just based on the integration of the current-time response, and adding corrections for the charge due to the double-layer charging (Q_{dl}) and the reaction of the adsorbed species (Q_i):

$$Q = \frac{2nFAcD^{1/2}t^{1/2}}{\pi^{1/2}} + Q_{dl} + Q_i \qquad (2.16)$$

Nevertheless, chronocoulometry offers important experimental advantages. First, unlike the current response that quickly decreases, the measured signal usually increases with time, and hence the later parts of the transient can be detected more accurately. Second, a better signal-to-noise ratio can be achieved. Third, contributions of charging/discharging of the electrochemical double layer and any pseudo-capacitance on the surface (charge consumed by the electrode reaction of adsorbed species (adsorption)) to the overall charge passed as a function of time can be distinguished from those due to the diffusing electro-reactants. A plot of the charge (Q) versus $t^{1/2}$, known as Anson plot, yields an intercept at t=0 that corresponds to the sum of Q_{dl} and Q_i (Figure 2.9b).

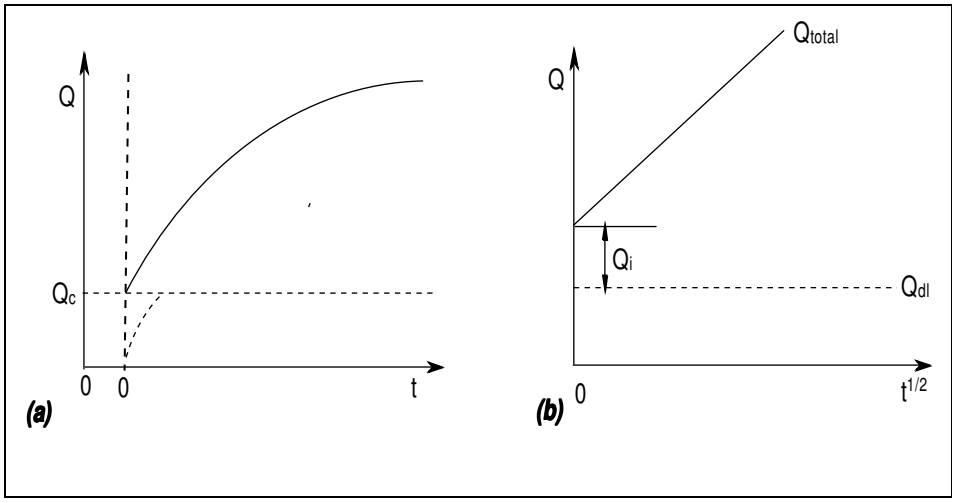

***Figure 2.9**: Chronocoulometric response (a) chronocoulometric charge vs. square root of time plot (b). Dashed curves in (a) displayed for the illustration of the capacitive charge effect, the dashed, horizontal line represents the charge response in the absence of reactant*

2.1.3. *Electrocatalysis*

Electrocatalysis is the catalysis of an electrode reaction.[32] The effect of electrocatalysis is an increase of the standard rate constant of the electrode reaction, which results in an increase of the Faradaic current. As the current increase can be masked by other non-electrochemical rate-limiting steps, the most straightforward indication for the electrocatalytic effect is the shift of the electrode reaction to a lower overpotential at a given current density. Electrocatalysis, as chemical catalysis, can be either homogeneous or heterogeneous in character. In homogenous electrocatalysis, both the catalyst and the substrate are in the same phase, commonly dissolved in the bulk solution, and the processes at the interface do not influence the chemical steps that involve it. In heterogeneous electrocatalysis, the catalyst is immobilized on the electrode surface, or the electrode itself plays the role of a catalyst.

MPc complexes exhibit catalytic activity for the electrochemical oxidation and reduction of a variety of target analytes in both homogeneous and heterogeneous phases.[33,34,35,36] These MPc electrodes act by lowering the overpotential of oxidation or reduction of the target analytes, and are known to mediate the redox process at the central metal and/or ring.[37,38] The mechanism for the electrocatalytic oxidation process due to the metal center is given by equation (2.17) and (2.18)

$$M^{(II)}Pc(-2) \longrightarrow M^{(III)}Pc(-2) + e^- \quad (2.17)$$

$$M^{(III)}Pc(-2) + A \longrightarrow M^{(II)}Pc(-2) + A_{ox} \quad (2.18)$$

For the electrocatalytic oxidation process due to the ring, equations (2.19) to (2.21) have been proposed.

$$MPc(-2) \longrightarrow [MPc(-1)]^{+\cdot} + e^- \quad (2.19)$$

$$2[MPc(-1)]^{+\cdot} \longrightarrow ([MPc(-1)]^{+\cdot})_2 \quad (2.20)$$

$$([MPc(-1)]^{+\cdot})_2 + A \longrightarrow MPc(-2) + A_{ox} \quad (2.21)$$

Scheme 2.1 shows an electrocatalytic reduction process promoted by MPc-based electrode. In this process, the MPc complex changes oxidation states upon interacting with the target analyte and it recovers its initial oxidation state by accepting or donating electrons to the electrode. The electrode simply acts as a source of electrons that are exchanged with the surface-confined MPc. Electrocatalytic activities are normally observed at potentials close to the formal potential of the MPc.

In this work, electrocatalytic oxidation of nitrite, thiocyanate, and formic acid and the reduction of oxygen at an edge plane pyrolytic graphite electrode modified with metallophthalocyanine complexes are investigated.

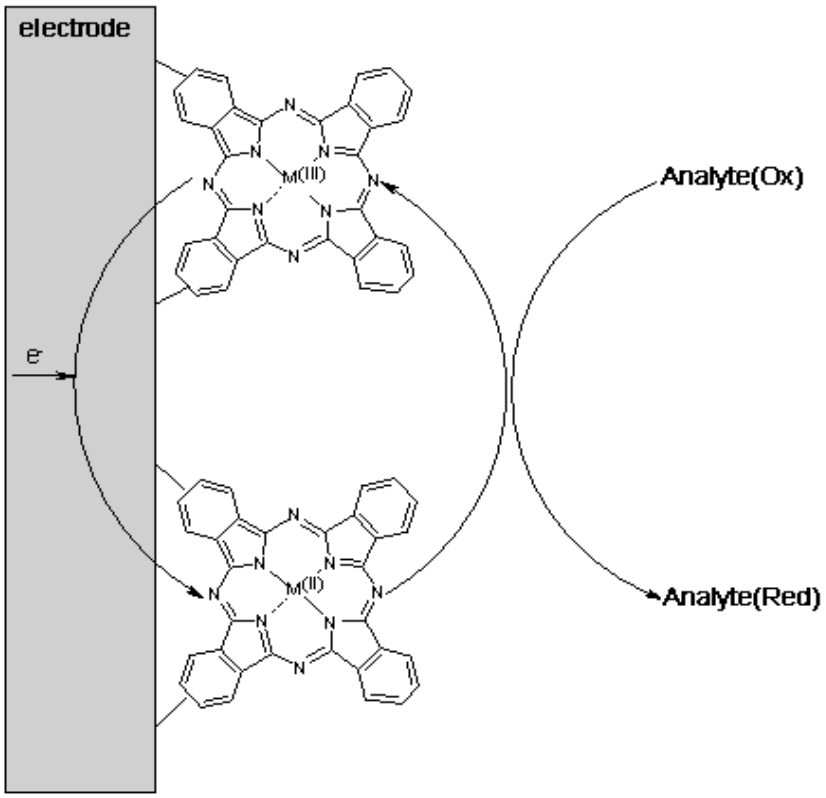

Scheme 2.1: *Schematic presentation of a catalytic process promoted by MPc electrode*[33]

2.1.4. *Electrochemical Impedance Spectroscopy*

Impedance spectroscopy is considered a powerful technique for investigating electrochemical systems and processes. Its strength lies in its ability to interrogate relaxation phenomenon, whose time constants range over several orders of magnitude.[39] The impedance technique is based on disturbing an electrochemical cell at equilibrium or steady state with alternating signal of small magnitude and measuring the current response. This disturbance can come from a

wide range of parameters such as applied potential, applied current, the convection rate at hydrodynamic electrodes, or light intensity. The applied disturbance is usually sinusoidal.

If the disturbance due to an applied voltage at a frequency (ω) to the electrochemical cell is considered:

$$V(t) = V_0 \sin \omega t \qquad (2.22)$$

where V (t) is voltage at time t, V_0 is the voltage amplitude, and ω is the radial frequency. The current response will take the form as in equation (2.23) with a phase shift denoted by θ

$$I(t) = I_0 \sin(\omega t + \theta) \qquad (2.23)$$

Where I (t) is the current at time t, I_0 is the current amplitude, and Φ is the phase shift. The impedance of the system is the ratio:

$$Z = \frac{V_t}{I_t} \qquad (2.24)$$

With a magnitude ($Z_0 = V_0/I_0$) and a phase shift (Φ) and thus present itself as a vector quantity. The complex notation for impedance will then be (Figure 2.10b):

$$Z = Z_0(\cos\theta + j \sin\theta) = Z' + j Z'' \qquad (2.25)$$

Where $j = \sqrt{(-1)}$, Z' is the real part and Z" is the imaginary part.

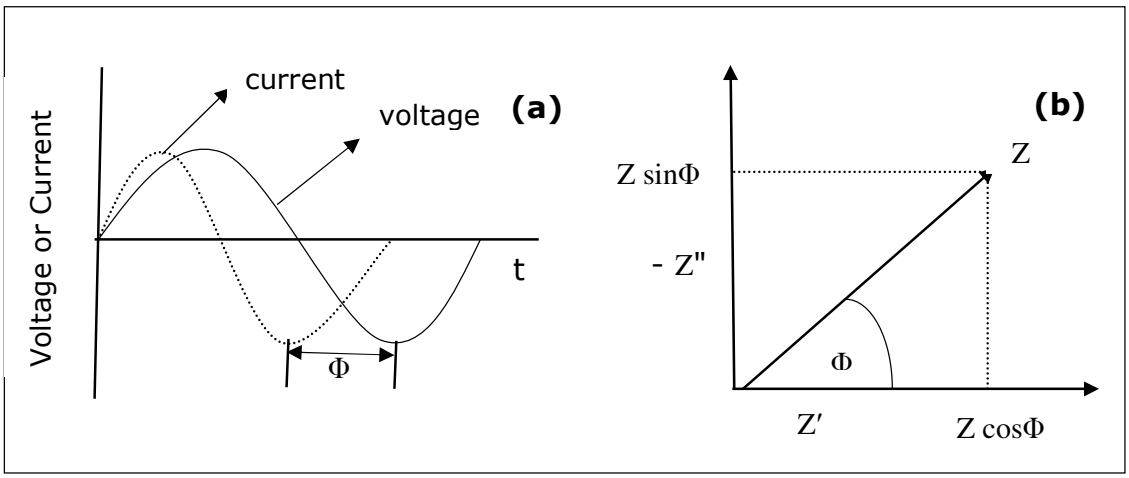

***Figure 2.10**: Sinusoidal voltage perturbation and current response (a), impedance presentation in the complex plane (b)*

2.1.4.1. *Data Presentation*

Graphical presentation of the measured impedance data are usually presented as 1) Nyquist or Complex plane plots (Figure 2.11(a)). It consists of plots of the real (Z') and imaginary (-Z") parts of the complex impedance (Z) as x and y axes, which are sometimes referred to as "resistance" and "reactance" respectively. As shown in Figure 2.11(a), the Nyquist plot for a simple charge transfer reaction is made of a semi-circle arc region at high frequencies lying on the x-axis followed by a straight line known as the Warburg impedance at low frequencies. The region of high frequencies is dominated by charge transfer at short times, while at high frequencies; diffusion plays the dominant role over a long time and the phase angle rises towards 45°. At high frequencies, diffusion of the reactants to and from the electrode is not important, because the currents are small and change

sign continuously.[2] Spectra as explained in Figure 2.11(a) can be used to extract information about electron transfer kinetics and diffusional characteristics. For fast electron transfer, the spectra will be completely overwhelmed by the Warburg, while for a sluggish electron transfer, a large semi-circle arc dominates. The diameter of the semi-circle arc equals the electron transfer resistance (R_{ct}). 2) Bode plots. This shows a plot of the phase angle and logarithm of the magnitude of impedance versus the logarithm of the frequency (Figure 2.11(b)). When resistive behaviour dominates the impedance behaviour, a horizontal line is observed in the presentation of log Z versus log f and a phase angle close to 0° is measured. When the impedance response is determined by a capacitance, a straight line with a slope of – 1 is observed and a phase angle of 90°, whereas diffusion-controlled phenomena (Warburg Impedance) would give a straight line with a slope of -1/2 and a phase angle of 45°.

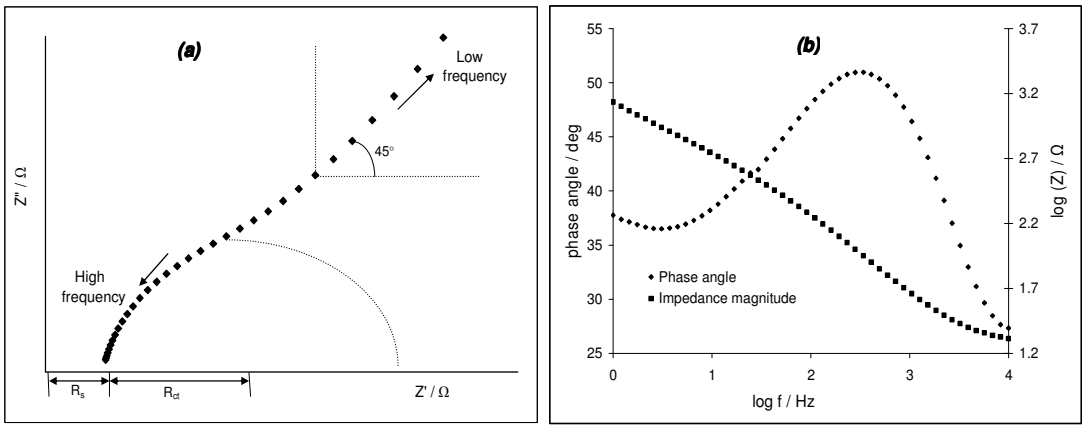

***Figure 2.11**: Nyquist (a) and Bode (b) plots for presentation of impedance data*

2.1.4.2. *Data Interpretation*

The measured data interpretation is usually carried out by the use of networks of electrical circuits called equivalent electrical circuits, selected based on the understanding of the electrochemical system. To model a simple three-electrode electrochemical cell in the presence of a diffusion related phenomena in terms of equivalent circuit, the Randles electrical equivalent circuit is employed (Figure 2.12). It consists of the resistance of electrolyte solution between the reference and working electrodes (R_s), the electrochemical double layer expressed as double-layer capacitance (C_{dl}), the impedance of the charge-transfer process (R_{ct}), and the Warburg impedance (Z_w) resulting from the semi-infinite diffusion of ions to the electrode surface.

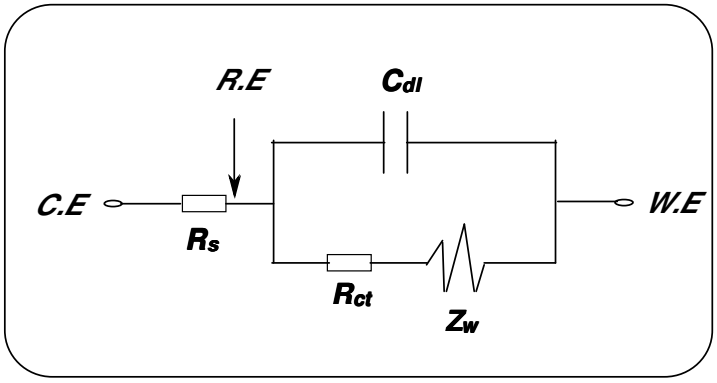

***Figure 2.12**: Classical Randles electrical equivalent circuit for an ideal behaviour*

Figure 2.12 describes a series arrangement of charge-transfer process (R_{ct}) and Warburg impedance (Z_w) that is in parallel

combination with the double-layer capacitance (C_{dl}), with the solution resistance (R_s) in series.

Figure 2.12 is made up ideal circuit elements such as resistors and capacitors, however, distributed circuit elements are required in addition to the ideal circuit elements to describe the impedance response of real systems adequately. In all real systems, some deviation from ideal behavior can be observed. If a potential is applied to a macroscopic system, the total current is the sum of a large number of microscopic current filaments, which originate and end at the electrodes.[36] If the electrode surfaces are rough or one or more of the dielectric materials in the system are inhomogeneous, then all these microscopic current filaments would be different. In a response to a small amplitude excitation signal, this would lead to frequency-dependent effects that can often be modeled with simple distributed circuit elements. One of these elements, which have found widespread use in the modeling of impedance spectra, is the so-called constant phase element (CPE). A CPE is defined as

$$Z_{CPE} = \frac{1}{[Q(j\omega)^n]} \tag{2.26}$$

where Q is the frequency-independent constant related to the interface, $j = \sqrt{-1}$, ω is the radial frequency, the exponent n arises from the slope of log Z versus log f (and has values $-1 \leq n \leq 1$). If n = 0, the CPE behaves as a pure resistor; n = 1, CPE behaves as a pure capacitor, n = –1 CPE behaves as an inductor; while n = 0.5

corresponds to Warburg impedance (Z_w) which is associated with the domain of mass transport control arising from the diffusion of ions. In short, CPE arises from several factors such as (i) the nature of the electrode (e.g., roughness and polycrystallinity), (ii) distribution of the relaxation times due to heterogeneities existing at the electrode/electrolyte interface, (iii) porosity and (iv) dynamic disorder associated with diffusion.[40] An electrical equivalent circuit describing the use of the constant phase element is shown in Figure 2.13.

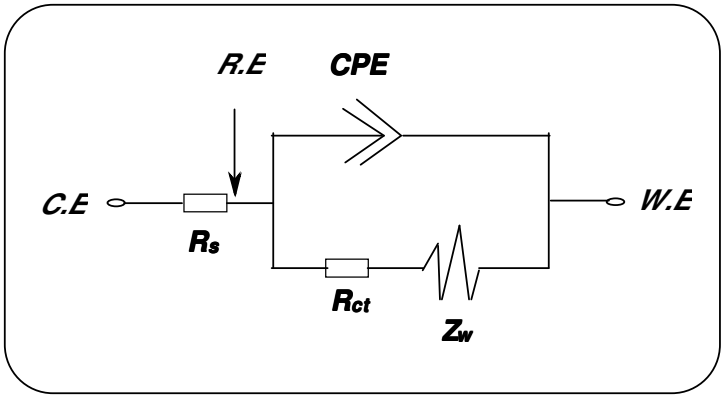

Figure 2.13: *Modified Randles equivalent circuit showing the CPE for non-ideal behaviour*

2.1.4.3. *Validation of Measurement*

To properly define an impedance measurement as a transfer function, the system under investigation has to fulfil the conditions of linearity, causality and stability during the measurement.[41] Most electrochemical systems are nonlinear as a result of current voltage at the electrode. Deviation from causality arises when the response is caused by the

concentration, current, or potential relaxation upon departure from equilibrium. Instrument artefacts or noise can also disturb causality. Continually changing corroded electrode does not guarantee stability of an electrochemical system.

To assess whether meaningful data that fulfils the above conditions have been obtained, a range of techniques and diagnostic tools have been developed to validate impedance data. One of the diagnostic tools employed in this work is the Kramer-Kronig test. The K-K tests are a series of integral equations that govern the relationship between the real and imaginary parts of complex quantities for systems fulfilling the conditions of linearity, causality, and stability. To assess whether experimental data fulfill the Kramer–Kronig tests,[36] one part of the impedance is calculated from the other part of the impedance, which has been experimentally determined. For example, the imaginary part can be calculated from the measured real part of the impedance .The calculated imaginary part of the impedance can then be compared with the measured imaginary part of the impedance. Any difference between calculated and measured values would indicate a deviation from one of the conditions of linearity, causality, or stability[36]. This method, however, requires that at least one part of the impedance is known between the frequency limits of zero and infinity. In most cases, the frequency range is not sufficiently large to integrate over the frequency limits zero and infinity. To overcome this problem,

various models for extrapolating the experimental data sets to the frequency limits have been suggested. One model employed is the fit of the impedance data with an equivalent electric circuit. Successful fit of such circuit to a data set is consistent with the Kramer-Kronig test.

2.2 Chemically Modified Electrodes

The IUPAC,[42] defined a chemically modified electrode (CME) as an electrode made of a conducting or semiconducting material that is coated with a selected monomolecular, multimolecular, ionic, or polymeric film of a chemical modifier and that by means of Faradaic (charge-transfer) reactions or interfacial potential differences (no net charge transfer) exhibits chemical, electrochemical, and/or optical properties of the film.

2.2.1. *General Methods of Modifying Electrode Surfaces*

Chemically modified electrodes are made by using one of the following methods:

2.2.1.1. *Chemisorption*

This is when molecules of modifying species are attached by valence forces. Included in this type of modification are the substrate-coupled self-assembled monolayers (SAMs) in which uncorrelated molecules spontaneously chemisorbed at specific sites on the surface of the electrode to form a superlattice.[43]

2.2.1.2. *Covalent Bonding*

Linking agents are used to covalently attach from one to several monomolecular layers of the chemical modifier to the electrode surface.

2.2.1.3. *Composite*

The chemical modifier is simply mixed with an electrode matrix material, as in the case of an electron-transfer mediator (electrocatalyst) combined with the carbon particles (plus binder) of a carbon paste electrode.

2.2.1.4. *Coating by thin films*

Electron-conductive and nonconductive thin films are held on the electrode surface by some combination of chemisorption and low solubility in the contacting solution or by physical anchoring in a porous electrode. CMEs covered with thin films are the most popular systems, because of their numerous advantages (simplicity of preparation, stability, well-defined or sizeable electrochemical responses). These thin films coated CMEs can be further divided according to the nature of the coating process:[39]

•**Cross-linking**. The chemical components are coupled to an electrode substrate to impart a desired property to the film.

•**Dip coating.** The electrode substrate is immersed in a solution for a given period of time, allowed to form film by adsorption, removed and allowed to dry.

•**Electrochemical deposition (redox deposition).** The electrode substrate is immersed in an electrolyte solution containing one or more dissolved salts or other ions that permit the flow of electricity and subjected to electrochemical treatment. Used in electroplating; by coating a conductive metal with a thin layer of material.

•**Electrochemical polymerization**. The electrode substrate is immersed in an approximately 1 mM concentrated solution of the modifier followed by repetitive voltammetric scanning within a specified potential window. The resulting voltammogram of the first scan is different from the subsequent scans indicative of the formation of the new species on the electrode surface.

•**Solvent evaporation (drop dry).** The droplet of the desired solution of volatile solvent such as dimethylformamide is applied to the electrode substrate and allowed to dry. A major advantage of this approach is that the modifier coverage is immediately known from the original solution concentration and droplet volume. This approach is used in this study.

•**Spin coating (spin casting).** As solvent evaporation, but electrode surface is rotated when excess amount of solution is applied. Rotation is continued while the fluid spins off the edges of the substrate, until the desired thickness of the film is achieved. The solvent used is usually volatile and simultaneously evaporates.

Coating by thin films can be a multi-step process, e.g., to produce multi-layered systems or to further functionalize and to improve

usability. More complex structures of CMEs also exist. They may contain more than one modifying substance, or more than one layer. Such a system can be called a micro- or nano-structured electrode, or integrated chemical system electrode.

2.3 Carbon Electrodes

Carbon is selected for many electrochemical applications because of its good electrical and thermal conductivity, low density, adequate corrosion resistance, low thermal expansion, low elasticity, and high purity. In addition, carbon materials can be produced in a variety of structures, such as powders, fibres, large blocks, thin solid and porous sheets, nanotubes, fullerenes, graphite, and diamond. Furthermore, carbon materials are readily available and are generally low-cost materials. There are three common forms of carbon: diamond, graphite, and amorphous carbon. All three are important for electrochemical applications.

2.3.1. *Diamond Electrode*

Diamond doped with boron is conductive, and hence can serve as a highly inert and robust electrode material. Indeed, there are many reports on the study of electrochemical reactions with boron-doped diamond electrodes.[44,45] Due to their exceptional chemical inertness and mechanical strength, diamond electrodes have been proposed for applications in extremely aggressive media such as strong acids.

2.3.2. *Graphite Electrode*

Graphite is the thermodynamically stable form of carbon under standard conditions.[46] Graphite has a gray metallic appearance, a density of 2.26 g cm^{-2}, and an atomic structure composed of graphene sheets, a two-dimensional honey comb structures of carbon atoms

(sp^2) where each atom has three nearest neighbours in 1.42 Å distance. In graphite, these sheets are stacked with a regular interlayer spacing of 3.35 Å. The structure of graphite allows electrons to move fast within graphene sheets. Graphite is widely employed as electrode material. A range of synthetic graphite materials have been developed such as carbon fibre electrodes, glassy carbon electrodes, carbon paste electrodes and highly oriented pyrolytic graphite electrodes (HOPG).

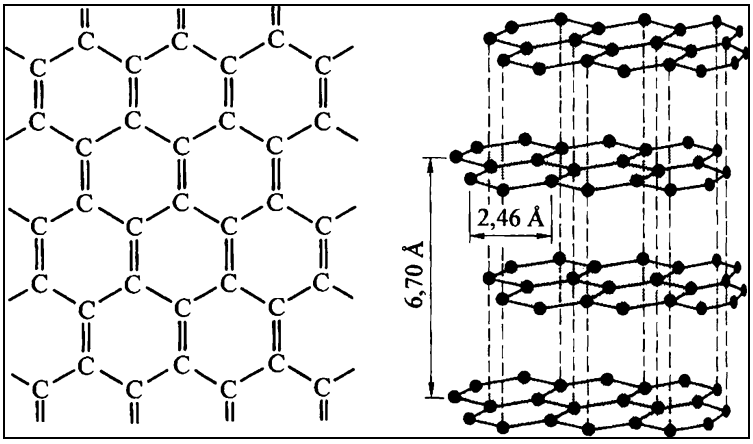

***Figure 2.14**: The structure of graphite electrode*[7]

- ***Carbon fibre electrode*:** Carbon fibre is produced by the carbonization of polyacrylonitrile at 1500 °C – 2500 °C to give highly electrically conducting fibres with 5-10 μm diameter with a carbon content >99%.Carbon fibre-based materials have found many applications due to their exceptionally high tensile strength. In electrochemistry carbon fibre used as microelectrodes are very important in analytical detection[47,48] and for in vivo electrochemical studies.[49,50]

- ***Glassy carbon electrode:*** Glassy carbon (also called vitreous carbon) is an advanced material of pure carbon combining glass-like mechanic characteristics with physical properties of graphite. Its structure comprises of interwoven ribbons of the graphite structure (Figure 2.15) with features of carbon that cannot be transformed into crystalline graphite even at temperatures of 3000°C.

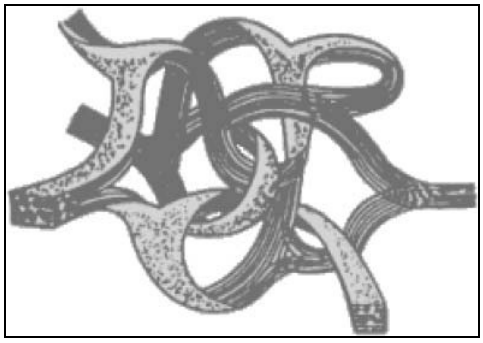

Figure 2.15*: Interwoven ribbons of graphite structure*[51]

In addition to the above-mentioned resistance to high temperature, it is also extremely resistive to many chemicals, it is impermeable to gases and liquids, has good electric conductivity, low density, high hardness, and high strength. Only strong oxidizing agents like oxygen at elevated temperature, or hot melts, or strong oxidizing acids can attack glassy carbon. But even under such conditions it is probably the most inert carbon material. Glassy carbon can be shaped to produce many forms thus it is widely used as an electrode material in electrochemistry. Surface pre-treatment is usually employed to create active and reproducible glassy carbon electrodes and to enhance

their analytical performance.[52] Such pre-treatment is usually achieved by polishing to a shiny mirror-like appearance with successively smaller alumina particles. The electrode is then rinsed with deionised water before use. The improved electron transfer capability has been attributed to the removal of surface contaminants, exposure of fresh carbon edges, and an increase in the density of surface oxygen groups.[53]

- ***Carbon paste electrode*:** Carbon paste electrodes have been described first by Adams in 1958.[54] He has used graphite powder mixed with a mulling liquid. As such for practical considerations liquids with low volatility, purity, and economy narrowed the choice to a few liquids like bromoform, bromonaphthalene, paraffin oil, silicone grease and Nujol. The paste is housed in a Teflon holder, contacted by a platinum wire, and occasionally a piston is used to renew the surface by extrusion of the used paste. Kuwana and French were the first to modify carbon paste electrodes with electroactive compounds[55] to measure the response of water insoluble compounds in an aqueous electrolyte solution. Later this approach has been expanded to study the electrochemical behaviour of inorganic insoluble compounds that may or may not be electron conductors.[56] Carbon paste electrodes have been developed in the last decades mainly to incorporate reagents and enzymes to prepare specific electrodes for analytical applications.[57,58,59] The long-term stability of the pastes is a problem,

as well as the fact that the binder can affect the electrochemistry of solid embedded particles.

- ***Highly oriented pyrolytic graphite electrode (HOPG)***: Highly oriented pyrolytic graphite (HOPG) is commercially produced by high temperature deposition of carbon at ceramic surfaces and graphitization at 3000°C.[60] Highly oriented pyrolytic graphite is employed as edge plane pyrolytic graphite electrode (EPPGE, graphene sheets perpendicular to the electrode surface) or as basal plane pyrolytic graphite electrode (BPPGE, graphene sheet parallel to the electrode surface) (Figure 2.16). The properties of these electrodes are very different due to the different abilities of electrons to transfer from the graphene edges or perpendicular to the graphite plane.[61] EPPGE is often observed to behave electrocatalytically[62] and has been successfully employed for processes involving immobilized redox proteins.[63] In this work the edge plane pyrolytic graphite electrode is employed.

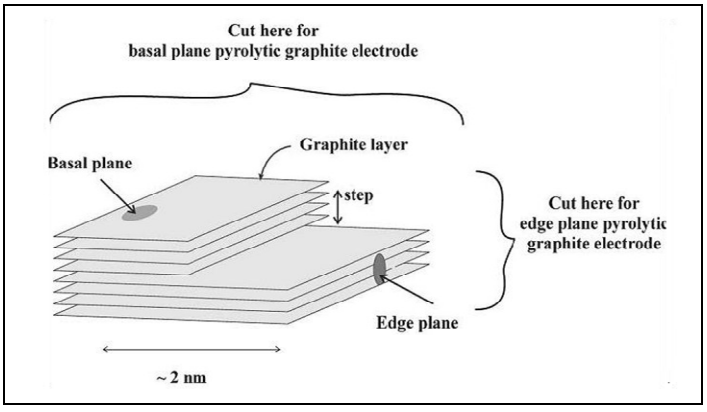

Figure 2.16*: Schematic representation of a step edge on a HOPG surface*[51]

Between the extremes of graphite and amorphous carbon there is a wide range of carbons with properties that can be tailored, to some extent, for a specific application by controlling the manufacturing conditions and subsequent treatments (heat treatment, chemical oxidation, etc.). Because of the wide variety of carbons that are available, there is a whole range of promising electrochemical applications for these materials, such as fuel cells, batteries, industrial electrochemistry, and electroanalytical chemistry. In fuel cells, carbon (or graphite) is an acceptable material of construction for electrode substrates, electrocatalyst support, bipolar electrode separators, current collectors, and cooling plates. Carbon and graphite are used in batteries as electrodes or as additives in order to enhance the electronic conductivity of the electrodes. As electrodes, graphites and disordered carbons reversibly insert lithium, and hence they may serve as the anode material in lithium batteries. Graphitic carbons intercalate lithium in a reversible multi-stage process up to LiC_6 and are used as the main anode material in commercial rechargeable Li ion batteries. As additives, carbon and graphite can be found in most of the composite electrodes of batteries, such as lithium and alkaline batteries. Flow batteries are also batteries where carbon and graphite can be found, both as electrodes and as bipolar separators. For the bipolar separators, nonporous carbon or graphite is required (for example, carbon–polymer composites, dense graphite, or other nonporous carbon such as glassy carbon). Activated carbon and

graphite are used as electrodes in these batteries, where the high surface area of these electrodes is used to store the electroactive species. Highly porous carbons can serve as electrodes in super (EDL = electric double layer) capacitors. Their very wide electrochemical window allows their use in nonaqueous (relative) high energy-high power density super (EDL) capacitors. A wide range of applications of carbon materials can be seen in what is termed industrial electrochemistry. These applications include the use of carbon electrodes in reactions involving inorganic compounds (e.g. chlorine evolution, ozone generation, etc.), the synthesis of organic materials using electrochemical methods, electrochemical treatment of solutions (removal and recovery of charged and uncharged species by electroadsorption and ion exchange in the porous structure of the carbon electrodes), and carbon capacitors, where the high and specific surface area leads to an extremely high double layer capacitance. Last, but not least, is the field of electroanalytical chemistry, in which carbon electrodes can be found. This field includes voltammetry, potentiometry, coulometry, etc., for measuring the concentration and detecting the presence of specific chemical species.

2.4 Carbon Nanotubes: General Introduction

Carbon nanotubes are made of sp^2-hybridized carbon atoms arranged in graphite type sheets building-up seamless hollow tubes capped by fullerene-type hemispheres. Their length ranges from tens of nanometers to several microns. They can be divided into two classes; single-walled carbon nanotubes (SWCNTs) and multi-walled carbon nanotubes (MWCNTs). SWCNTs consist of single hollow tubes with diameter 0.4 to 2 nm. They can be metallic conductors or semiconductors. The conductivity depends on their chirality, presence of catalytic particles, ion doping, and functionalisation. MWCNTs are composed of concentric tubes. Their diameter ranges from 2 to 100 nm and they can be regarded as metallic conductors. Both classes of carbon nanotubes are already recognized as attractive electrode material.

2.4.1. *Historical Perspective*

The history of carbon nanotubes have generated a lot of controversy as to who is/were to be given credit for the discovery of carbon nanotubes. While some authors[64] credited Radushkevich and Lukyanovich[65], others[48] credited Wiles and Abrahamson[66] and more recently Peter Harris in his book[67] credited Iijima[68] for producing better carbon nanotubes than those that have been previously produced catalytically, and differed from them in being all-carbon structures,

closed at both ends, and not 'contaminated' with catalyst particles. The current explosion of interest in carbon nanotubes only came after the rediscovery by Iijima. The uncertainty surrounding the question of who actually discovered nanotubes probably explains why no Nobel Prizes have yet been awarded in this area.

2.4.2. *Structure of Carbon Nanotubes*

Carbon nanotubes appear as sheets of graphite cells that have been mended together to look almost like a latticework fence and then rolled up in a tube shape (Figure 2.18). Although this is a simple explanation for the look of the structure of carbon nanotubes, this is not how carbon nanotubes are created, nor does it explain their immense strength or other incredible structural abilities. Carbon nanotubes are typically around two millimeters in length or less but have the capability, if formed correctly, of being more than one hundred times stronger than steel.

Carbon nanotubes are capable of being formed in both single walled structures, also known as Single Walled Carbon Nanotubes (SWCNTs) (Figure 2.17a) and multiple walled structures, also known as Multi-Walled Carbon Nanotubes (MWCNTs) (Figure 2.17b). Each structure of carbon nanotubes has its own set of properties that make it appropriate for different uses across science, architecture, geology,

agriculture and engineering, among the many fields carbon nanotubes have become useful for.

Single walled carbon nanotubes have electric properties that are not present in multi-walled carbon nanotubes due to the makeup of their structure. These single walled structures can be used in large quantities for thermal purposes. Additionally, the electric properties of these macro miniature carbon nanotubes make them perfect for engineering electronics to even smaller than their current "nano" sized status. Although they do not share the same electric properties in the structure of carbon nanotubes as single walled carbon nanotubes, multi walled carbon nanotubes have their place in science and exhibit several properties that are more useful than single walled carbon nanotubes for a variety of applications. For instance, the makeup of multi-walled carbon nanotubes makes them perfect for use in the medical field. The medical field utilizes multi-walled carbon nanotubes in the production of sensors for medical diagnostics. Biosensors are able to detect microscopic amounts of biological or chemical agents, which help to diagnose an illness much quicker. Multi-walled carbon nanotubes are used for these purposes because of their electrochemically advanced properties, which are due in part to their double or multi walled structures.

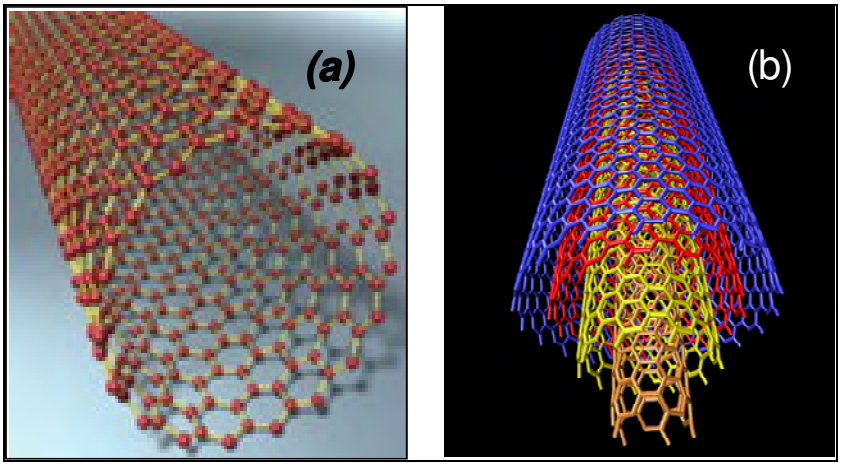

Figure 2.17: *Geometric structures of (a) SWCNT and (b) MWCNT*

In addition to the two different basic structures, there are three different types of carbon nanotubes that are possible. These three types of carbon nanotubes are armchair carbon nanotubes, zigzag carbon nanotubes and chiral carbon nanotubes.

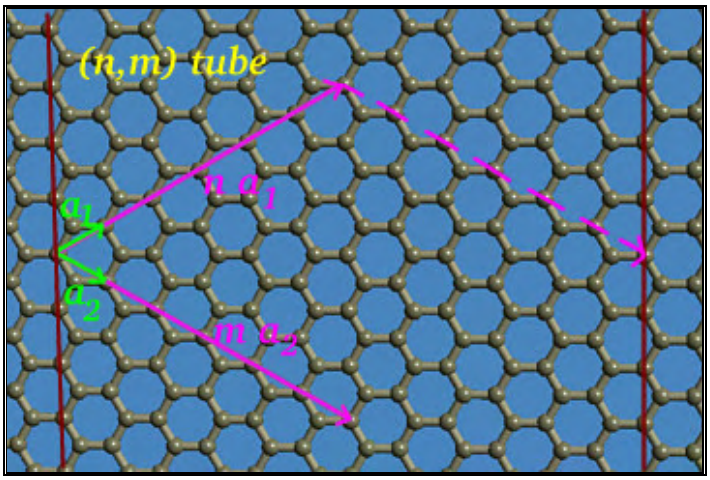

Figure 2.18*: Unit cells of carbon nanotubes*

The difference in these types of carbon nanotubes are created depending on how the graphite is "rolled up" during its creation process. The structure is expressed in terms of one-dimensional unit

cell, defined by the vector where a_1 and a_2 are unit vectors, and n and m are integers. A nanotube constructed in this way is called an (n,m) nanotube. Rolling up the sheet along one of the symmetry axis gives either a zig-zag (m=0) tube or an armchair (n=m) tube. It is also possible to roll up the sheet in a direction that differs from a symmetry axis to obtain a chiral nanotube. Each structure of carbon nanotubes in these three varieties is different and has different implications for science.

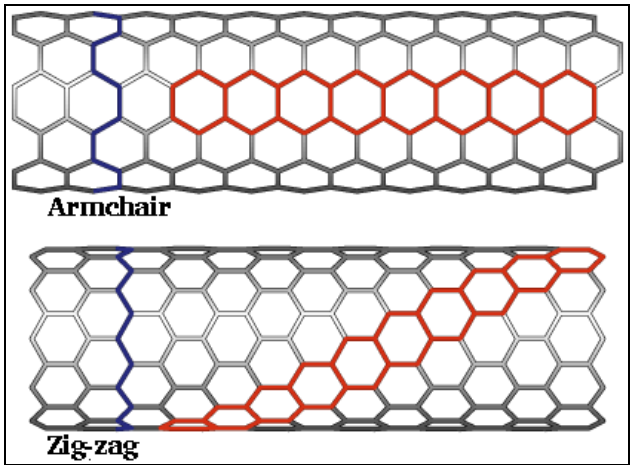

***Figure 2.19**: The types of carbon nanotubes created from how the graphene sheet is rolled*

2.4.3. *Synthesis of Carbon Nanotubes*

SWCNTs and MWCNTs are usually made by d.c. electric-arc discharge, high temperature heat treatment, laser vaporisation, or catalytic chemical vapour deposition.[64] The two most popular methods are the arc discharge and the chemical vapour deposition. The arc

discharge method produces carbon nanotubes of the best quality whereas the chemical vapour deposition method can produce more carbon nanotubes. These synthesis methods for carbon nanotubes introduce high concentration of impurities. The carbon-coated metal catalyst contaminates the nanotubes of the HiPco route, and both carbon-coated metal catalyst and, typically, ~60% forms of carbon other than nanotubes are formed in the carbon-arc route.[69,70] Harsh acid treatment is used to remove these impurities, which introduce other impurities, can degrade or shorten nanotube length and perfection, and adds to nanotube cost. Nevertheless, the acid treatment was used in this project to shorten the tubes and introduce the carboxyl groups.[71]

2.4.4. *General Applications of Carbon Nanotubes*

Potentially carbon nanotubes have varied applications in fields such as nanotechnology, electronics, optics, materials science and architecture. The superior mechanical properties of CNTs offers structural application ranging from clothes, sport gears and space elevators,[72] while from its electronic properties, nanotube based transistors have been made.[73] As paper battery,[74] produced from a thin sheet of cellulose infused with aligned carbon nanotubes. The nanotubes act as electrodes; allowing the storage devices to conduct electricity. The battery, which functions as both a lithium-ion battery

and a supercapacitor, can provide a long, steady power output comparable to a conventional battery, as well as a supercapacitor's quick burst of high energy.

Currently, the application of carbon nanotubes has been limited to the use of bulk nanotubes. Bulk CNTs have already been used as composite fibres in polymers to improve the mechanical, thermal and electrical properties of the bulk product. In solar cells,[75] ultracapacitors,[76] and nanoelectromechanical systems.[77,78] Nitrogen-doped carbon nanotubes may replace platinum catalysts used to reduce oxygen in fuel cells.[79]

2.5 Metallophthalocyanines: General Introduction

2.5.1. *Historical Perspective*

According to history, an unidentified blue compound, which we now know as metal-free phthalocyanine, was described in 1907.[80] In 1927, Swiss researchers accidentally synthesized copper phthalocyanine, copper naphthalocyanine, and copper octamethylphthalocyanine in an attempted conversion of *o*-dibromobenzene into phthalonitrile. They remarked on the enormous stability of these complexes but did not further characterize these blue complexes.[81] The same blue product was further investigated at Scottish Dyes, Ltd., Grangemouth, Scotland (later ICI) in 1928.[82] The phthalocyanines are intensely coloured and are used as dyes.[83,84,85]

2.5.2. *Structure of Metallophthalocyanines*

Phthalocyanine is a planar, 18 π-electron, tetradentate dianionic ligand that binds metals through four inwardly projecting nitrogen centres to form metallophthalocyanine complex (Figure 2.20). Metallophthalocyanines are structurally related to other macrocyclic pigments such as porphyrin; both consist of four pyrrole-like subunits linked to form a 16-membered ring. The pyrrole-like rings within the phthalocyanine are closely related to isoindole. Ring-substituted derivatives in the peripheral and non peripheral positions are also possible. The central atoms of MPc can carry additional ligands.

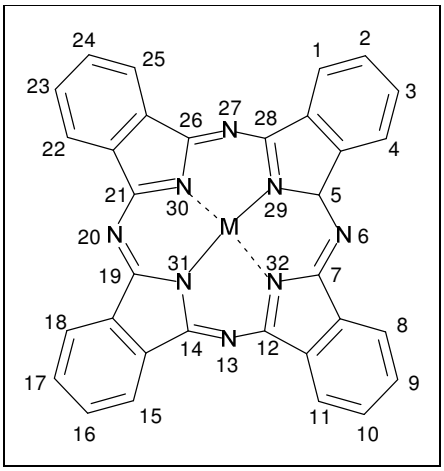

Figure 2.20: *Geometric structure of metallophthalocyanine*

2.5.3. *Synthesis of Metallophthalocyanines*

Metallophthalocyanines can be prepared according to the following synthetic routes[86,87] as shown in Scheme 2.2. It generally involves heating a mixture of metal salt (or metal) with a desired precursor, which might be phthalonitrile or diiminoisoindole (which are referred to as the classical precursors; others include phthalic anhydride, o-cyanobenzamide and phthalimide etc), in the presence of various reagents to form the MPc. For high purity MPc, the phthalonitrile route is preferred, while for large volume the phthalic anhydride route is employed.[88] Another synthetic route which is fast and eliminates the use of solvents is the microwave irradiation[89,90]

The strong intermolecular cohesion of unsubstituted MPc makes it a non-melting insoluble solid; introduction of substituents on the phthalocyanine ring drastically changes their basic properties[91,92]

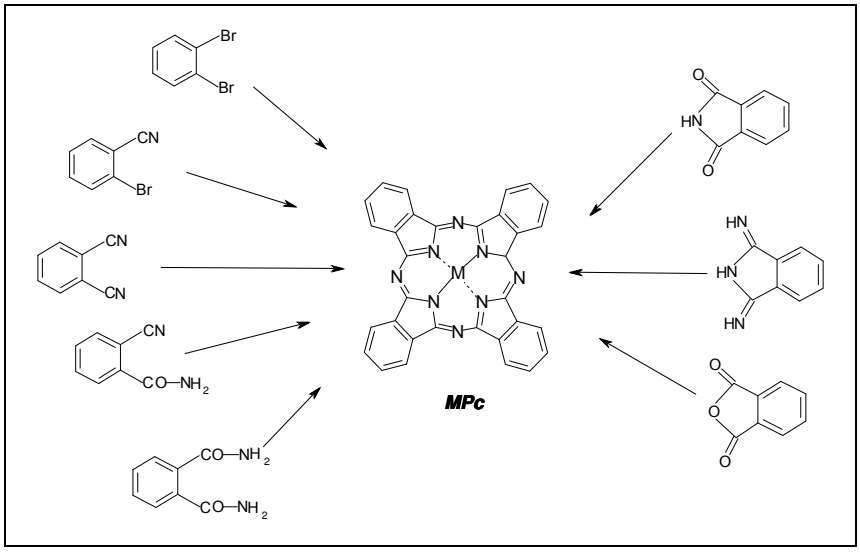

Scheme 2.2: *General synthetic routes for Metallophthalocyanines*

Cyclotetramerisation of the appropriate substituted phthalonitrile derivative is used to obtain a substituted MPc. Synthetic routes for the synthesis of peripherally and non-peripherally octasubstituted MPc derivatives which are usually obtained from the disubstituted phthalonitrile and the metal salt[88,93] is shown in Scheme 2.3. This route was used in the preparation of the peripherally octasubstituted butylsulphonyl derivative (MOBSPc, where M = Co or Fe) described in this thesis. The octacarboxymetallophthalocyanine described in this thesis was obtained from its amide intermediate product, tetra-amidometallophthalocyanine (MTAPc) using pyromellitic anhydride and DBU as a catalyst[94] (Scheme 2.4).

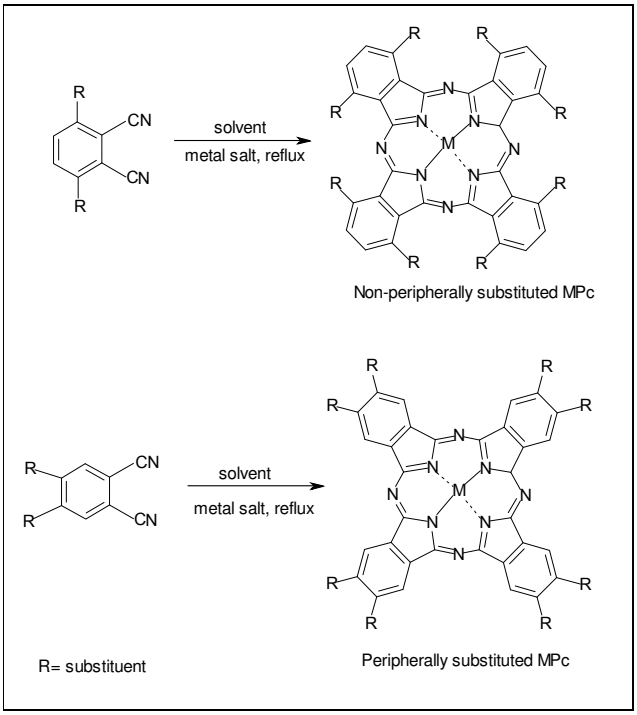

Scheme 2.3: *Synthetic routes for peripherally and non-peripherally substituted MPc*

The introduction of an axial ligand onto an appropriate cation held within the central cavity of the MPc give rise to an axial-ligated MPc. This is obtained by refluxing the uncoordinated MPc in a coordinating solvent or other axial ligands (Scheme 2.5).[95,96]

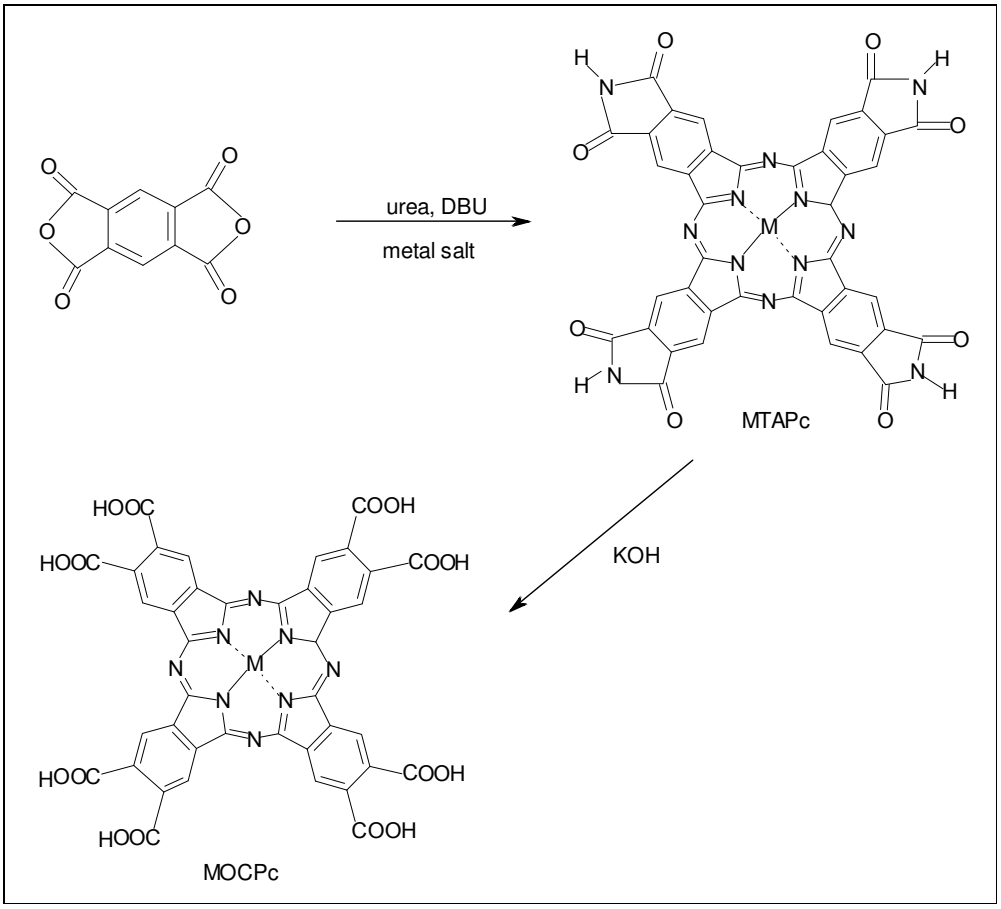

Scheme 2.4: *Synthetic route for octacarboxy-metallophthalocyanine*[91]

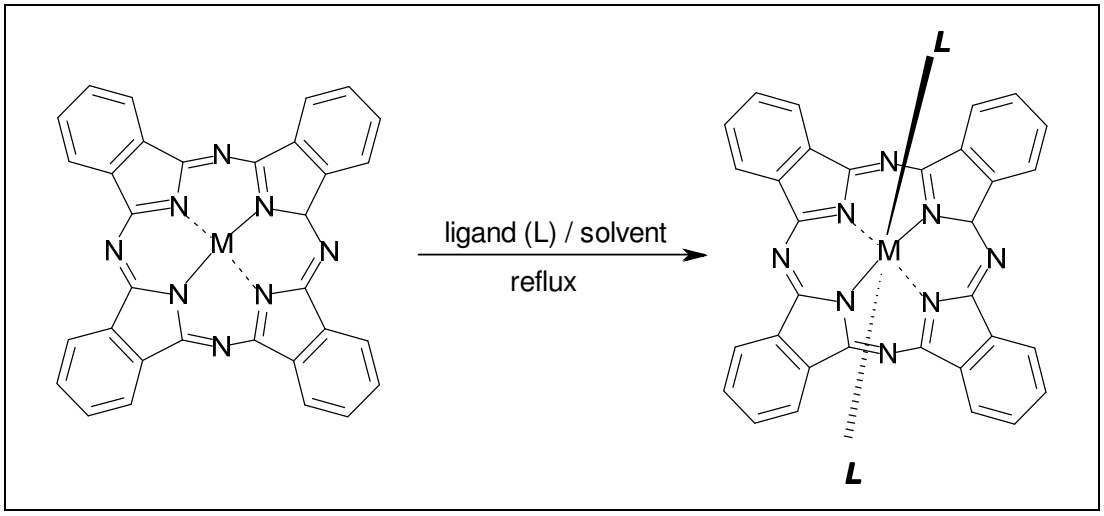

Scheme 2.5: *Synthetic route for axial-ligated MPcs*[92,93]

2.5.4. *Electronic Absorption Spectra of Metallophthalocyanines*

The typical absorption spectra of MPc complex are shown in Figure 2.21 (A). It consist of an intense absorption peak appearing at the red end of visible region around 600 – 700 nm known as the Q band and a less intense peak at the blue end around 300 – 400 nm known as the B or Soret band. These peaks are characteristics of MPc complexes, however, MPcs can also show intense absorption peaks at the near infra-red region (700 – 1,300 nm).[97] Both bands are due to π → π* transitions within the delocalized phthalocyanine ring system[98,99,100]

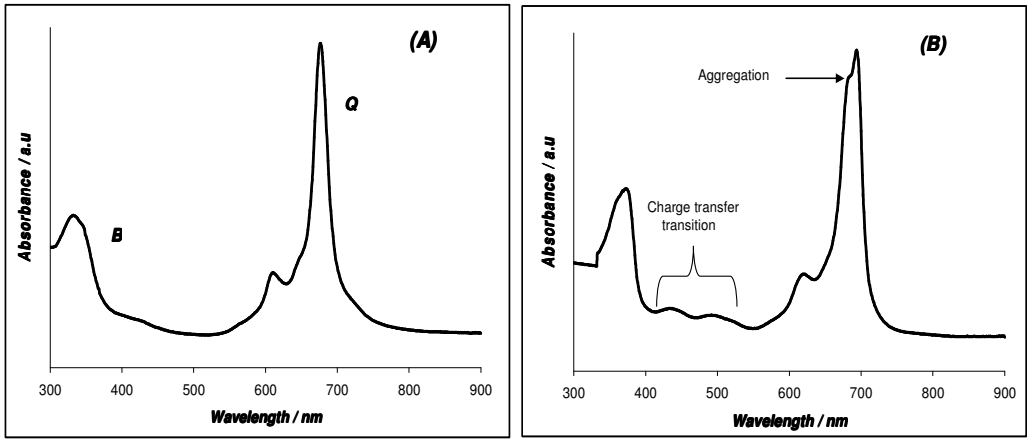

Figure 2.21: *Typical electronic absorption spectra of phthalocyanine showing the B and Q bands (A) and the charge transfer transition (B)*

The Gouterman's four-orbital model[101] depicted in Scheme 2.6 describes the transitions as the transfer of electrons from the highest occupied molecular orbital (HOMO) (π) to the lowest unoccupied molecular orbital (LUMO) (π*). The B band consists of two transitions

arising from the HOMO a_{2u} and b_{2u} to LUMO e_g, while the Q band transition arises from HOMO a_{1u} to LUMO e_g orbital[96]

As shown in Figure 2.21(B) other absorption bands might be observed in the spectra of MPc, these bands are known as charge transfer transition (CTT). The d orbital of the transition metal may lie between the HOMO and LUMO of the phthalocyanine ligand (Scheme 2.6), consequently a possible charge transfer transition may take place either by metal to ligand (MLCT) or ligand to metal (LMCT). These bands appear as weak absorption peaks occurring at the near infra-red region or between the B and Q bands in the 300 – 400 nm regions[96,102,103] The following are known to affect the position of the absorption bands in phthalocyanines, especially the Q band: central metal, axial ligation, solvents, peripheral and non-peripheral substituents, aggregation and ring extension.[94]

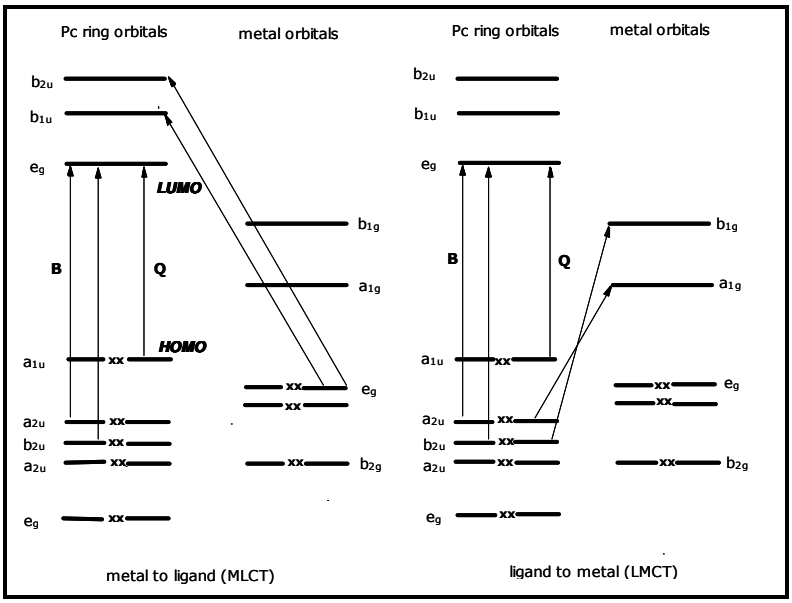

Scheme 2.6: *Gouterman's four – orbital model*[97]

2.5.5. *Electrochemical Properties of Metallophthalocyanines*

The functions of metallophthalocyanine complexes are mostly based on their electron transfer reactions because of the π electron conjugated ring system. It is of vital importance that the electron transfer behaviour (redox process) of MPcs is interrogated in solution in order to study further application. This redox process is usually observed using electrochemical or spectro-electrochemical methods.[96,104] Neutral MPc exists as a dianion (Pc^{-2}),[105] which may be successively oxidised or reduced at the MPc ring, the metal centre or both.

2.5.5.1. *Ring Process*

$[MPc^{-1}]^{+}$and $[MPc^{0}]^{2+}$ cation radicals are formed when the MPc dianion is oxidised by loss of one or two electrons respectively from the HOMO. As shown in Scheme 2.7, a hole is created in the a_{1u} level which allows for a transition from the low-lying e_g level,[97] leading to the formation of $[MPc^{-1}]^{+}$. Loss in intensity of the Q band, formation of weak bands in the 700 – 825 nm region and a broad band near 500nm characterises the presence of $[MPc^{-1}]^{+}$. MPc^{-3}, MPc^{-4}, MPc^{-5} and MPc^{-6} species are formed when the phthalocyanine ring is reduced by gaining successively one to four electrons at the LUMO.[102,106]

2.5.5.2. *Metal Process*

Redox processes may or may not take place at the central metal ion of the MPc. This redox process is due to the interaction between the phthalocyanine ring and the central metal. It is well known that the first row transition metals of various MPcs differ from those of the main group MPcs due to the fact that the metal d orbitals may be positioned between the HOMO and the LUMO of the neutral Pc ligand.[101,103,107,108] The first oxidation and first reduction processes occur at the metal centre of the MPc only for Mn, Fe and Co derivatives, depending on factors within the environment such as solvent, electrolyte, axial ligands and ring substituents. For Ni, Cu and Zn derivatives, redox processes occur only on the Pc ring. Redox process at the metal centre is characterised by a shift in the Q band without much reduction in intensity.[109]

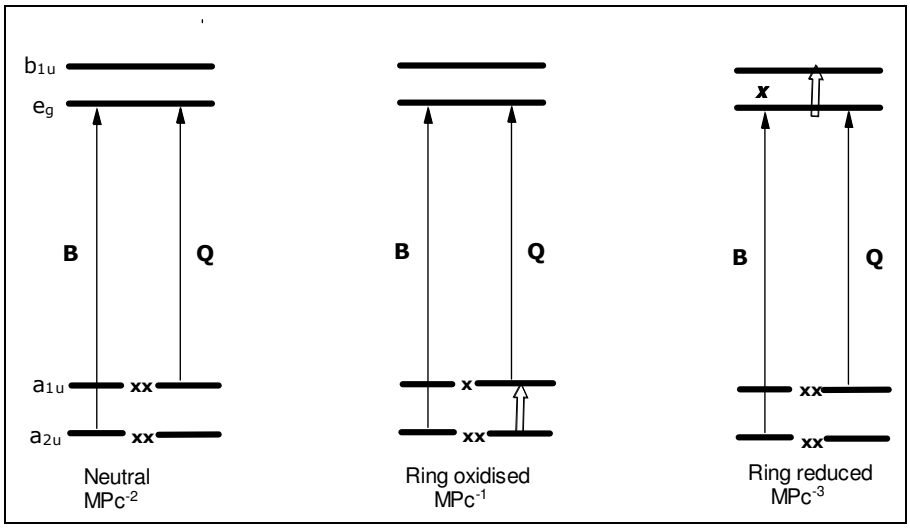

Scheme 2.7: *Energy level diagram of one-electron ring oxidised and one-electron ring reduced MPc complex*[97]

The redox properties of a given MPc complex is determine by the nature of the central metal, axial ligands, solvents and the substituents on the periphery of the ring. Electron-withdrawing substituents such as sulphonyl groups, decreases the electron density of the ring and the central metal, thereby making it easier to reduce and difficult to oxidise MPc complexes, and vice versa for electron donating substituents. Furthermore, redox processes occurring at the central metal or ring results in colour changes, with ring redox processes showing more drastic colour changes. New peaks are formed on oxidation or reduction of the Pc ring because of transitions[97] (Scheme 2.7).

2.5.6. *General Applications of Metallophthalocyanines*

The phthalocyanines are a remarkable class of macrocyclic compounds possessing interesting physical and chemical properties, with their areas of application stemming from these properties. Due to their excellent thermal and chemical stability, beautiful bright colours, high tinctorial strength and fastness to light,[85,110] they have mainly found application as dyestuffs for jeans and other clothing, and as pigments in pens, plastics and metal surfaces. More recently, they have found applications in the printing, photocopying and electrophotography industry; thermal writing display, solar cells, fuel

cells, molecular electronics, electronic and chemical sensors, catalysis, photodynamic therapy and optical data storage devices.[85,107,111,112,113] New applications of phthalocyanine complexes are reported on a constant basis.

2.6 Overview of Target Analytes

2.6.1. *Oxygen Reduction Reaction (ORR)*

Oxygen, with the molecular formula O_2, sometimes referred to as dioxygen, is of fundamental importance in biological processes of energy conversion such as breathing and aerobic metabolism.

Oxygen reduction reaction as an electrochemical process has been extensively studied.[114,115,116] The reasons for such interest in this reaction are (i) its fundamental significance with respect to electrode kinetics, (ii) its role in the area of electrochemical energy conversion and corrosion.

In electrochemical energy conversion, oxygen reduction in aqueous solutions is considered to proceed via two overall reaction pathways:

The direct four electron pathway:

$$O_2 + 4H^+ + 4e^- \rightarrow 2H_2O \text{ (acidic)} \qquad 1.23 \text{ V (SHE)} \qquad (2.27)$$

$$O_2 + 2H_2O + 4e^- \rightarrow 4OH^- \text{ (alkaline)} \qquad 0.40 \text{ V (SHE)} \qquad (2.28)$$

The peroxide pathway:

$$O_2 + 2H^+ + 2e^- \rightarrow H_2O_2 \xrightarrow{(2H^+ + 2e^-)} 2H_2O \text{ (acidic)} \qquad 0.70 \text{ V (SHE)} \qquad (2.29)$$

$$O_2 + H_2O + 2e^- \xrightarrow{-OH^-} HO_2^- \xrightarrow{(H_2O + 2e^-)} 3OH^- \text{ (alkaline)} \qquad -0.07 \text{ V (SHE)} \qquad (2.30)$$

The two reaction pathways may also take place in parallel. These pathways are usually determined by the structure of the catalyst used to catalyze the reaction, the reaction conditions and the nature of the electrode upon which the catalyst is adsorbed. Electrodes that promote

the 4e^- reduction of oxygen to water are Ag,[117] Pt[118] and the Pt family metals.[119] Platinum is considered to be the best and most expensive electrocatalyst for oxygen reduction, since the reduction on this electrode is known to occur with the lowest potential.[120] Electrodes that promote the 2e^- reduction of oxygen to water are Au,[121] Hg[122] and various carbon materials.[123]

The mode of adsorption of molecular oxygen on the metal surface also determines the reaction pathway. Three different models for adsorption have been proposed; the Griffiths model,[124] the Pauling's model,[125] and the bridge model.[126,127]

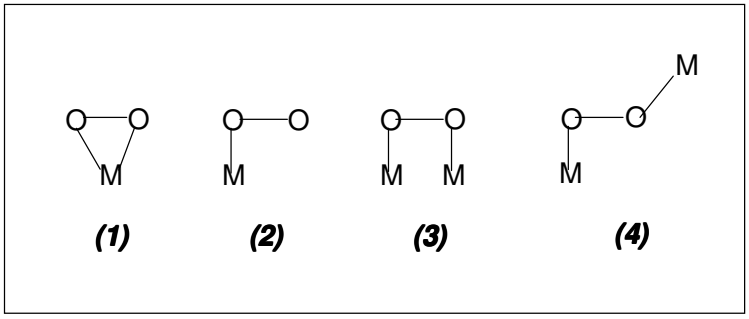

Scheme 2.8: *Possible adsorption mechanism of oxygen on a metal complex*

The Griffiths model **(1)** involves a side-on interaction of oxygen with the metal. The bonding can be viewed as arising from two contributions: a σ type bond formed by the overlap between a mainly π orbital of oxygen and dz^2 (and s) orbital on the metal and a π back bond interaction between the metal dπ orbitals and the partially occupied π* antibonding orbital on oxygen.

The Pauling model **(2),** an end-on interaction of oxygen with the metal forming an angle close to 120° is proposed. In this model, a σ – rich orbital of oxygen donates electron density to an acceptor orbital dz^2 on the metal forming a σ – type bond. A π interaction is also produced between the metal dπ (dxz, dyz) orbital's and π* on oxygen, with charge transfer from the metal to the oxygen molecule. This model favours the $2e^-$ reduction of oxygen to peroxide. The principal difference between the Griffiths and Pauling model is the steric factors and the nature of the σ bond formed. They both exhibit strong σ donation of an electron pair from oxygen but with different donor orbital's being considered.

The Bridge model **(3)** was proposed by Yeager[123,124] and is likely to occur on noble metals such as Pt where oxygen is reduced to water with little or no peroxide formed. This type of interaction promotes the rupture of the O-O bond, favouring the direct $4e^-$ reduction of oxygen to water. The Griffith type of interaction could also lead to the rupture of O-O bond. The bridge model can also occur as a *trans* form **(4)**.

The ORR is a multi-electron reaction that may include a number of elementary steps involving different reaction intermediates. Of the various reaction schemes proposed, the simplified version of the scheme given by Wroblowa and co-workers [128](Scheme 2.9) appears to be the most effective one to describe the complicated reaction pathway by which oxygen is reduced at metal surfaces:

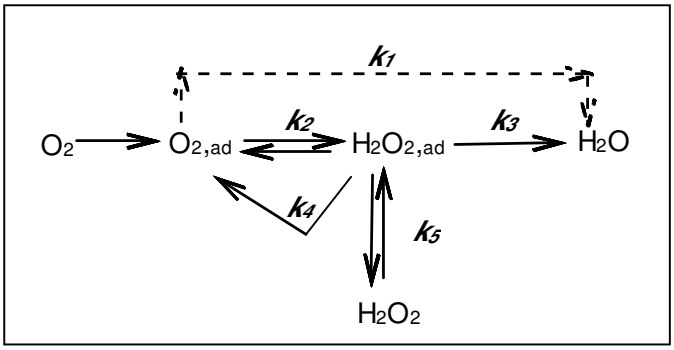

***Scheme 2.9**: Series-parallel reaction scheme for oxygen reduction*[125]

On the basis of this reaction scheme, oxygen can be electrochemically reduced either directly to water with the rate constant k_1 (direct 4*e*- reduction) or to H_2O_{2ad} with rate constant k_2 (peroxide pathway). The adsorbed peroxide can be electrochemically reduced to water with the rate constant k_3, catalytically/chemically decomposed on the electrode surface k_4, or decomposed into the bulk of the solution k_5.

The main problem in the development of an efficient electrochemical energy conversion device (fuel cell) is in the sluggish ORR kinetics even on the most catalytically active electrode material. Transition metal MPc complexes, notably the iron-centred (FePc) and cobalt-centred (CoPc) phthalocyanine complexes have been intensively reported as possible alternative electrocatalysts for the ORR. FePc complexes are preferred to their CoPc counterparts as their ORR activities occur at low potentials, following the direct 4-electron process that result to water as the main reduction product.[129,130] Several reports have shown that MPc complexes integrated or supported on

carbon nanotubes (CNTs) greatly enhance the electrocatalytic performance of the electrode.[131] However, the use of such MPc for ORR is limited. There are other reports involving metalloporphyrins (MPs) and CNTs.[132,133] It is well established that MPc and MPs are structurally different and, expectedly, exhibit contrasting physico-chemical properties. In this study the impact of co-immobilising MPc complexes with acid functionalized MWCNT for ORR activity is explored.

2.6.2. *Formic Acid Oxidation*

Research into formic acid (FA) has received great attention and has been considered as a replacement candidate for methanol as fuel in fuel cells. This is due to its high electrochemical activity arising from its non-toxicity, non-flammability and its ability to facilitate the transport of proton within the anode catalyst.[134,135] Because of its advantages over methanol, a direct formic acid fuel cell (DFAFC) is being gradually recognised as a promising power source.[136]

Platinum is one of the most frequently used catalyst for formic acid oxidation,[137,138] however, previous studies have shown that practical applicability is inadequate because the electro-oxidation process on a platinum catalyst surface could occur through two parallel pathways, the "direct pathway" and the "CO pathway"[139,140]. In the "direct pathway" which is preferred, the formic acid is oxidized directly to CO_2:

$$HCOOH + Pt \longrightarrow X \longrightarrow CO_2 + 2H^+ + 2e^- \quad (2.31)$$

where X is an active intermediate with relatively short lifetimes[136]. However, the formic acid is oxidized slowly in the "CO pathway", because a poisoning intermediate CO_{ad} will be formed before the end product CO_2 is yielded.

$$HCOOH + Pt \longrightarrow Pt\text{-}CO + H_2O \quad (2.32)$$

$$Pt + H_2O \longrightarrow Pt\text{-}OH + H^+ + e^- \quad (2.33)$$

$$Pt\text{-}CO + Pt\text{-}OH \longrightarrow 2Pt + CO_2 + H^+ + e^- \quad (2.34)$$

$$\text{Overall: } HCOOH \longrightarrow CO_2 + 2H^+ + 2e^- \quad (2.35)$$

The CO_{ad} intermediate formed in the CO pathway can be strongly adsorbed on the surface of the Pt, thereby poisoning the catalyst, hence not desirable. Unfortunately, various studies indicate that the electro-oxidation on common Pt catalysts occurs mainly through the CO pathway[141,142] In order to lead the reaction to the desired "direct pathway", the Pt-based bimetallic catalysts (Pt-M), such as PtSn[134,143,144] PtGe,[134,135,136] PtPb,[134] PtAs,[134] PtBi,[133] and PtRu[145] were redesigned and tested. It was found that bimetallic catalyst performed much better than pure Pt catalyst.[135,136,146]

On the other hand, the use of Pt catalyst integrated with metal macrocyclic compounds (such as MPc) for the oxidation of formic acid is virtually unknown. The only closest work in this area is the work by Zhou *et al.*[147] who carried out the electro-oxidation of formic acid using a bulk Pt disc electrode modified with water-soluble iron(II)

tetrasulphophthalocyanine (FeTSPc) complex. The obvious disadvantages of such system include (i) the high cost of Pt bulk metal support and (ii) the high probability of the immobilised FeTSPc to be easily washed off from the electrode during operation due to its high solubility in aqueous solution. Therefore, it is important to explore low content Pt systems that contain FePc complexes that are not water soluble (hydrophobic system) and supported on a low-cost carbon electrode substrate. In this work, it is shown that hydrophobic PtFeOCPc can serve as potential electrocatalyst for the oxidation of formic acid in acidic medium.

2.6.3. *Thiocyanate Oxidation*

Thiocyanate (SCN^-) is considered less toxic than cyanide hence is found in many industrial and biological applications, for instance its concentration in mining effluent is not regulated at the present time.[148] However, thiocyanate is known to decompose and form cyanide when exposed to ultraviolet radiation, it is then possible that sunlight may liberate cyanide to levels toxic to aquatic life from effluent rich in thiocyanate and has been known to block the iodine uptake by thyroid gland .In view of this consideration, it is not unlikely that in the future some limit may be imposed on the concentration of thiocyanate in effluents. The presence of thiocyanate in body fluids as a detoxification product of hydrogen cyanide (HCN),[149] has been used to monitor

hydrogen cyanide from tobacco smoke, fire atmospheres, and some vegetables that contain cyanogenic glucosides.[150] Electrodes modified with MPcs have been reported as efficient potential electrochemical sensors for the determination of thiocyanate. Electrochemical detection of thiocyanate with MPc based sensors is best performed in acidic conditions (between pH 4 and 5)[151] and the oxidation of SCN^- catalysed by horseradish peroxidase, an FePc-like molecule, occurs optimally at pH 4.0, hence this study was carried out in pH 5 phosphate buffer conditions.[152,153]

2.6.4. *Nitrite Oxidation*

Nitrite (NO_2^-), has been known for centuries and is still been used as a preservative[154] due to its anti-microbial activity. It is a color-enhancing agent to cured meat products and also provides indirect beneficial effect on flavour.[155] When ingested it react with haemoglobin, leading to reduction in the blood oxygen-carrying capacity, and with amines converting them into nitrosamines, which are well known carcinogenic substances. The build – up of nitrite concentrations in the environment, owing to their use in agricultural processes (as fertilizers), resulting in contamination of water sources for human consumption, has been of major concern.[156] Hence, it is almost impossible not to encounter nitrite ions or the products of their use in our everyday domestic activities. Various researchers have

suggested strategies to facilitate the detection, determination and monitoring of nitrite.[145,157] Intensive studies have been carried out in the electrocatalytic behaviour and detection of nitrite using MPc complexes.[158,159] The electrochemical detection of nitrite is best performed in neutral pH phosphate buffer solution,(pH 7.4), this is because nitrite exist as nitrite ion (NO_2^-) in neutral phosphate buffer solution but disproportionate to produce neutral nitric oxide (NO) in slightly acidic conditions,[160] hence this study was carried out in phosphate buffer pH 7.4.

2.7 Microscopic and Spectroscopic Techniques

Wealth of macroscopic information can be obtained about the processes occurring at the electrode-solution interface with the electrochemical methods so far discussed, however, to obtain microscopic information about the structure of an electrode surface requires the use of microscopic methods since the surface of a solid in contact with a liquid phase usually differs substantially from the interior of the solid both in chemical composition and physical properties. Some of the microscope and spectroscopic methods used in this work to characterise an electrode surface are scanning probe microscopy (SPM), which consist of the scanning tunnelling microscope (STM) and atomic force microscope (AFM). For the purpose of this study the AFM technique was employed. Others are scanning electron microscope (SEM), transmission electron microscope (TEM), energy dispersive spectroscopy (EDS), and X-ray diffraction (XRD).

2.7.1. *Atomic Force Microscopy (AFM)*

Atomic force microscopy is one of the two techniques of scanning probe microscopy used for imaging of sample surfaces. The AFM was invented in 1986[161], and relies on raster scanning to probe sample properties at or near the surface (typically several nanometers deep) and immediately above the surface (typically up to several tens of nanometers high). Raster scanning is performed with actuators whose

motion can be incremented in small steps and with high precision. These actuators are usually made of piezoelectric materials shaped into the form of a hollow tube, or they are made of a mechanical flexures or a hybrid of both. Raster scanning makes it possible to record the probe-sample interaction point-by-point. For each x, y coordinate pair, the interaction is recorded as one data point. The collection of these data points is then synthesised into the SPM image, a 3-D map. The most common images are the topography images (Figure 2.22). The AFM imaging is made possible when a flexible force-sensing cantilever with a sharp tip at the end is scanned in a raster pattern over the surface of the sample. During a scan, the force on the tip is held constant by the up and down motion of the tip, which then provides the topographic information. Two modes are operational with AFM; the contact mode and the tapping mode.

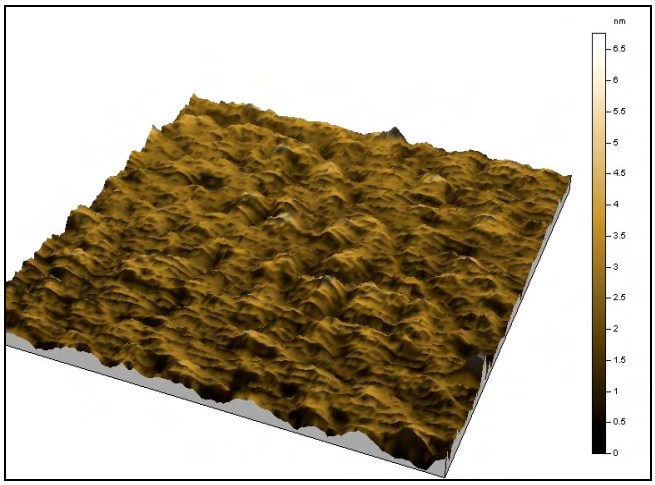

Figure 2.22: *AFM 3-D topographical image of iron(II) pthalocyanine on glassy carbon plate*

2.7.2. *Scanning Electron Microscopy (SEM)*

The scanning electron microscope (SEM) produces high resolution images of a sample surface in high vacuum.[162] The samples must be clean, dry, and electrically conductive. Scanning of the sample surface is achieved with a beam of energetic electrons in a raster pattern focused to a spot with a diameter in the range of some nanometer. When the electrons penetrate the sample, they interact with the atoms up to a depth of some micrometer releasing several signals such as backscattered electrons, Auger electrons, elastically scattered electrons, characteristic and bremsstrahlung X-rays, and secondary electrons from the surface. The backscattered and secondary electrons which serve as the basis of SEM originate within a few nm from the surface due to their low energy and are detected by photomultipliers to form a two-dimensional image of the surface with a lateral resolution down to 1 nm. The brightness of the signal depends on the number of secondary electrons. Morphological and topographical information is extracted that is necessary in understanding the behavior of surfaces; hence SEM examination is the first step in the study of surface properties of solids.

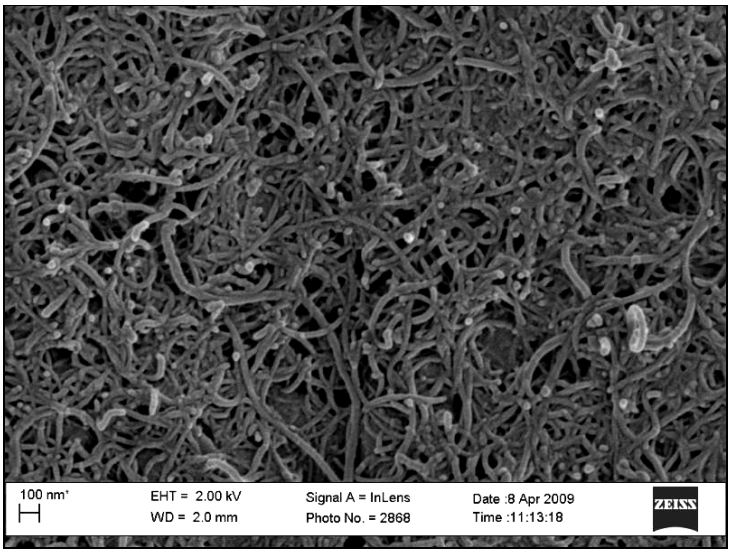

Figure 2.23: *High resolution SEM image of multi-walled carbon nanotubes*

2.7.3. *Transmission Electron Microscopy (TEM)*

The transmission electron microscope was first built by Max Knoll and Ernst Ruska in 1931 and was commercially available in 1936 with the microscope having a resolving power greater than that of light. Transmission electron microscopy is a microscopy technique that uses beam of energetic electrons generated by thermionic emission from a filament. The electrons interact with the ultra thin sample as it passes through. An image is formed from this interaction; magnified and focused onto an imaging device.[163] A TEM is composed of several components, which include a vacuum system in which the electrons travel, an electron emission source for generation of the electron stream, a series of electromagnetic lenses, as well as electrostatic plates. Also required is a device to allow the insertion into, motion within, and removal of specimens from the beam path. Imaging

devices are subsequently used to create an image from the electrons that exit the system. TEMs are capable of imaging at a significantly higher resolution due to the small *de Broglie* wavelength of electrons. This allows for examination of single columns of atoms which are in the region of nanometers, hence it has found application in nanoscience and nanotechnology research.[164]

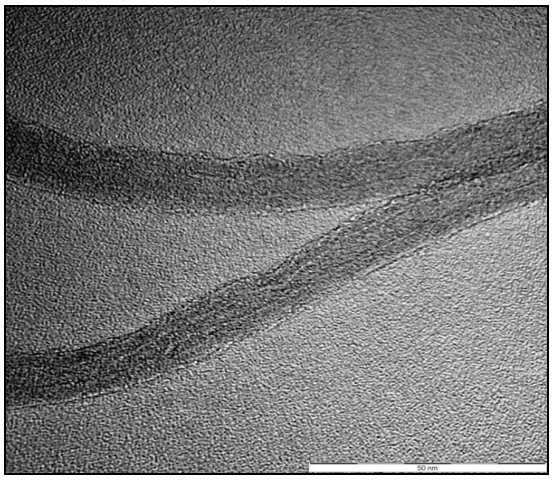

Figure 2.24: *TEM image of multi-walled carbon nanotubes*

2.7.4. *Energy Dispersive X- Ray Spectroscopy (EDS)*

EDS is an analytical capability that can be coupled with applications such as SEM and TEM. When beam of electrons interact with a sample surface, variety of emissions including X-rays are produced[165]. An energy-dispersive (EDS) detector is used to separate the characteristic x-rays of different elements into an energy spectrum, and EDS system software is used to analyze the energy spectrum in order to determine the abundance of specific elements. EDS can be used to find the

chemical composition of materials down to a spot size of a few microns, and to create element composition maps over a much broader raster area.

EDS systems include a sensitive x-ray detector, a liquid nitrogen dewar for cooling, and software to collect and analyze energy spectra. The detector is mounted in the sample chamber of the main instrument at the end of a long arm, which is itself cooled by liquid nitrogen. The most common detectors are made of Si (Li) crystals that operate at low voltages to improve sensitivity. The detector contains a crystal that absorbs the energy of incoming x-rays by ionization, yielding free electrons in the crystal that become conductive and produce an electrical charge bias. The x-ray absorption thus converts the energy of individual x-rays into electrical voltages of proportional size; the electrical pulses correspond to the characteristic x-rays of the element. A typical EDS spectrum is portrayed as a plot of x-ray counts vs. energy (in keV). Energy peaks correspond to the various elements in the sample. Generally they are narrow and readily resolved, but many elements yield multiple peaks. For example, iron commonly shows strong K_{α} and K_{β} peaks. Elements in low abundance will generate x-ray peaks that may not be resolvable from the background radiation.

2.7.5. *X-Ray Diffraction (XRD)*

X-ray diffraction is a unique method for studying the phase composition and atomic structure of crystalline materials. The method is based on the X-ray (neutron or electron) reflection from the atomic planes. The reflection angle θ depends on the X-ray wave length λ and the distance d between the atomic planes (Bragg's Law):

$2d \sin \theta = n\lambda$ (n = integer) (2.36)

The positions (angles) and intensities of the reflections in the diffraction patterns are fingerprint for each compound and can be transformed into the atomic arrangement.

The samples for the crystal structure determinations are usually single crystals, but more complex modern methods allow such an analysis for powder materials. The X-ray powder diffraction patterns are widely used to identify the type of material in any mixture by comparing them with the standard patterns of the International Powder Diffraction File (PDF) database.[166]

References

1. A.J Bard, L.R Faulkner, *Electrochemical Methods*, 2nd edition, Wiley, New York, (2001)

2. W. Schmickler, *Interfacial Electrochemistry*, Oxford University Press, Inc, New York (1996)

3. J.O'M Bockris, S.U.M Khan, *Surface Electrochemistry*, Plenum, New York, (1993)

4. H Bach, F Baucke, D Krause, *Electrochemistry of Glasses and Glass Melts, Including Glass Electrodes*, Schott Series, Springer, Berlin (2000)

5. T Osaka, M Datta, *Energy Storage for Electronics*, Gordon and Breach Science Publ. (2000)

6. P.M.S. Monk, *Fundamentals of Electroanalytical Chemistry*, John Wiley and Sons Ltd, Chichester, New York (2001)

7. A.J. Bard, G. Inzelt, F. Scholz (Eds), *Electrochemical Dictionary*, Springer, Berlin (2008)

8. J. Wang, Analytical *Electrochemistry*, VCH Publishers Inc. New York (1994)

9. D.B. Hibbert, *Introduction to Electrochemistry*, Macmillan, London (1993)

10. C. Kittel, *Thermal Physics*, 3rd edition, Wiley, New York (1969)

11. G. Inzelt, *Kinetics of Electrochemical Reactions*. In: F. Scholz (ed) *Electroanalytical Methods,* Springer, Berlin (2000)

12. K.B Oldham, J.C Myland, *Fundamentals of Electrochemical Science*, Academic Press, San Diego,(1994)

13. H.A Laitinen, I.M Kolthoff, *J Phys Chem* **45** (1941), 1061

14. H.A Laitinen, I.M Kolthoff, *J Phys Chem* **45** (1941), 1079

15. R.S Nicholson, I Shain, *Anal Chem* **6** (1964), 3706

16. F. Marken, A. Neudeck, A.M Bond, *Cyclic Voltammetry* In: F Scholz (ed) *Electroanalytical Methods*, Springer, Berlin, (2000)

17. D.K Gosser, *Cyclic Voltammetry: Simulation and Analysis of Reaction Mechanisms*, VCH, New York, (1993)

18. J. E. B. Randles, *Trans. Faraday Soc*. **44** (1948) 327

19. R. S. Nicholson, I. Shain, *Anal. Chem*. **36** (1964) 1351

20. A. Sevcik, *Coll. Czech*. *Chem. Comm*. **13** (1958) 349

21. J.A. Harrison, Z.A. Khan, *J. Electroanal. Chem*. **28** (1970) 131

22. J. Wang, *Analytical Electrochemistry*, 3rd ed, Wiley-VCH John Wiley & Sons Publishers Inc., Hoboken, New Jersey (2006).

23. E. R. Brown, R. F. Large, *in Physical Methods of Chemistry, Vol.1-Part IIA:Electrochemical Methods*, eds. A. Weissberger and B. Rossiter, Willey-Interscience, New York (1971).

24. R.G. Compton, C. E. Banks, *Understanding Voltammetry*, World Scientific Publishing Co. Pte. Ltd (2007).

25. J. Ni, H. Ju, H. Chen, D. Leech, *Anal. Chim. Acta* **378** (1999) 151

26. R. D. Rocklin, R. W. Murray, *J. Phys. Chem.* **85** (1981) 2104

27. C.M.A. Brett, A.M.O. Brett, *Step and Pulse Techniques* in A.J. Bard, M. Stratmann, P.R. Unwin (Eds), *Encyclopedia on Electrochemistry*, vol 3, Wiley-VCH, Weinheim, Germany (2008)

28. J. A. Turner, J. H. Christie, M. Vukovic, R. A. Osteryoung, *Anal. Chem*. **49** (1977) 1904

29. G. C. Barker, A. W. Gardner, *J. Electroanal. Chem*. **100** (1979) 641

30. P. H. Rieger, *Electrochemistry*, Prentice Hall, Oxford (1987)

31. A. J. Bard (ed) *Electroanalytical Chemistry*, Marcel Dekker, New York 13 (1994)

32. F.G. Banica, A. Ion, *Electrocatalysis-based Kinetic Determination*. In: R.A Meyers (ed) *Encyclopaedia of Analytical Chemistry*. Wiley, Chichester, 11115, (2000)

33. J.H. Zagal, S. Griveau, J.F. Silva, T. Nyokong, F. Bedioui, *Coord. Chem. Rev.,* (2010) in press

34. T. Mugadza, T. Nyokong, *Electrochim. Acta*, **55** (2010) 2606

35. W. Lu, N. Li, W. Chen, Y. Yao, *Carbon*, **47** (2009) 3337

36. H-s. Yin, Y-l. Zhou, S-y. Ai, *J. Electroanal. Chem*. **626** (2009) 80

37. J. Oni, T. Nyokong, *Anal. Chim. Acta*, **432** (2001) 9

38. J. H. Zagal, *Coord. Chem. Rev.,* **119** (1992) 89

39. S.Krause, *Impedance Method* In: A.J. Bard, M. Stratmann, P.R. Unwin (eds), *Encyclopaedia on Electrochemistry*, vol 3, Wiley-VCH, Weinheim, Germany (2008)

40. M.E. Orazem, B. Tribollet, *Electrochemical Impedance Spectroscopy,* John Wiley & Sons Inc, Hoboken, NJ, (2008)

41. C. M. Brett, A. M. O. Brett, *Electrochemistry: Principle, Methods and Applications*, Oxford University Press, New York, USA (1993).

42. R.A. Durst, A.J. Baumner, R.W. Murray, R.P. Buck, C.P. Andrieux, *Pure & Appl. Chem.*, **69** (1997), 1317

43. D.L. Allara, *Biosens. Bioelectronics* **10** (1995), 771

44. E.R. Sartori, R.A. Medeiros, R.C.Rocha-Filho, O. Fatibello-Filho, *Talanta* **81** (2010) 1418

45. S.C.B. Oliviera, A.M.Oliviera-Brett*, Electrochim. Acta* **55** (2010) 4599

46. A.F Holleman, N Wiberg, *Inorganic Chemistry*, Academic Press, London, (1995)

47. H. Kuramitz, M. Matsushita, S. Tanaka, *J. Watres*., **38** (2004) 2331

48. G. Munteanu, S. Munteanu, D.O. Wipf, *J. Electroanal. Chem*., **632** (2009) 177

49. M-F. Suaud-Chagny, *Methods* **33** (2004), 322

50. L. Xiang-Qin, K. Guang-Feng, C. Ying, *Chin J Anal Chem*, **36** (2008) 157

51. C.E. Banks, R.G. Compton, *Analyst*, **131** (2006), 15

52. R.C. Engstrom, *Anal.Chem*. **56** (1984)

53. R.L. McCreery, *Carbon electrodes: Structural effects on electron transfer kinetics,* in A.J. Bard, (ed), *Electroanalytical Chemistry* , vol. 18, Marcel Dekker, New York, (1991)

54. R.N Adams, *Anal Chem* **30**, (1958), 1576

55 . T. Kuwana, W.G. French, *Anal Chem* **36**, (1964), 241

56. F Scholz, B Meyer, *Voltammetry of Solid Microparticles Immobilized on Electrode Surfaces*. In: A.J. Bard, I Rubinstein (eds) *Electroanalytical Chemistry*, vol. 20. Marcel Dekker, New York, (1998)

57. I. Švancara, K. Vytřas, J. Barek, J. Zima, *Crit Rev Anal Chem* **31** (2001), 311

58 . L. Gorton *Electroanalysis* **7** (1995),23

59. K. Kalcher, J.M. Kauffmann, J. Wang, I. Švancara, K. Vytřas, C. Neuhold, Z. Yang *Electroanalysis* **7** (1995), 5

60. H.O Pierson, *Handbook of carbon, graphite, diamond and fullerenes,* Noyes Publications, New Jersey, (1993)

61. R.L. McCreery, Carbon electrodes: Structural effects on electron transfer kinetics, in A.J. Bard, (ed), *Electroanalytical Chemistry* , vol. 17, Marcel Dekker, New York, (1991)

62. C.E. Banks, R.G. Compton, *Anal Sci* **21** (2005),1263

63. L.S. Conrad, H.A.O. Hill, N.I. Hunt, J. Ulstrup, *J. Electroanal. Chem*. **364** (1994), 17

64. M. Monthioux, V.L. Kuznetsov, *Carbon* **44** (2006) 1621

65. L.V Radushkevich, V.M Lukyanovich, *Zurn Fisic Chim*, **26** (1958) 88

66. P.G. Wiles, J. Abrahamson *Carbon* **6** (1978) 341

67. P.J.F. Harris, *Carbon Nanotube Science*, Cambridge University Press, New York, (2009)

68. S. Iijima, *Nature* **354** (1991) 56

69. S. H. Lai, Y. L. Chen, L. H. Chan, Y. M. Pan, X. W. Liu, H. C. Shih, *Thin Solid Films* **444** (2003) 38

70. S. G. Louie, *Top. Appl. Phys*. **80** (2001) 113

71. J. Liu, A. G. Rinzler, H. Dai, J.H. Hanfer, R.K. Bradley, P.J. Boul, A. Lu, T. Iverson, K. Shelimov, C.B. Huffman, F. R. Macias, Y. S. Shon, T.R. Lee, D.T. Colbert, *Science* **280** (1998) 1253

72. B.C. Edwards, *The Space Elevator*. BC Edwards, ISBN 0974651710, (2003)

73. H.W.C. Postma, T. Teepen, Z. Yao, M. Grifoni, C. Dekker, *Science* **293** (2001) 76

74. "Beyond Batteries: Storing Power in a Sheet of Paper Eurekalert.org. August 13, 2007. http://www.eurekalert.org

75. "New Flexible Plastic Solar Panels Are Inexpensive And Easy To Make". ScienceDaily, July 19, 2007.http://www.sciencedaily.com

76. MIT LEES on Batteries, MIT press release, 2006

77. T. Simmons, D. Hashim, R. Vajtai, P.M. Ajayan, *J. Am. Chem. Soc.* **129** (2007) 10088

78. "Hot nanotube sheets produce music on demand", *New Scientists News*, 31 October 2008

79. Chemical & Engineering News, 9 February 2009, "Nanotube Catalysts", p. 7

80. A. Braun, J. Tcherniac, *Berichte der Deutschen Chemischen Gesellschaft,* **40** (1907), 2709.

81. H. de Diesbach, E. von der Weid, *Helevtica Chimica Acta*, **10** (1927), 886

82. J. M. Robertson, *J. Chem. Soc.* (1936) 1195

83. C. C. Leznoff, A.B.P. Lever (eds), *The Phthalocyanines*, vols 1-4, Wiley, (1986-1993)

84. N. B. McKeown, *Phthalocyanine Materials - Synthesis, Structure and Function*, Cambridge University Press, New York, (1998)

85. K. Kadish, K. M. Smith, R. Guilard (eds), *The Porphyrin Handbook*, Vols. 15-20, Academic Press, (2003)

86. C.C. Leznoff, in *Phthalocyanine: Properties and Applications*, C.C. Leznoff, A.B.P. Lever (eds), Vol 1, VCH Publishers, New York, (1989)

87. R.B. Linstead, A.R. Lowe, *J. Chem. Soc*., (1934), 1022

88. P. Gregory, *J. Porphyrins Phthalocyanines*, **3** (1999), 468

89. D.M. Maree, T. Nyokong, *J. Chem. Res*. (S), (2001), 68

90. E. Ç. Kaya, H. Karadeniz, H. Kantekin, *Dyes and Pigments* **85** (2010), 177

91. D. Wohrle, V. Schmidt, *J. Chem. Soc. Dalton Trans*. (1988), 549

92. D. Schlettwein, N.R. Armstrong, *J. Phys. Chem.*, **98** (1994), 11771

93. M. Hanack, P.Haisch,, H. Lehman, *Synthesis*, (1993), 387

94. K. Sakamoto, E. Ohno, *Prog. Org. Coating*, **31** (1997), 139

95. J. Metz, M. Hanack, *J. Am. Chem. Soc.,* **105** (1983), 829

96. T. Nyokong, *J. Chem. Soc., Dalton Trans*., (1993), 3601

97. T. Nyokong, *Electronic Spectra, and Electrochemical Behaviour of Near Infra-red Absorbing Metallophthalocyanines*. In: J. Jiang (ed), *Functional Phthalocyanine Molecular Materials*, vol 135, (2010)

98. L. Boucher, *Coordination Chemistry of Macrocyclic Compounds*, G.A. Melson (ed) Plenum Press, (1979)

99. T. Nyokong, M.J. Stillman, In: C. C. Leznoff, A.B.P. Lever (eds), *Phthalocyanines: Properties and Applications,* VCH Publishers, New York, Vol 1, (1989)

100. A.B.P. Lever, *Adv. Inorg. Radiochem*., **7** (1965), 28

101. M. Gouterman, In: D. Dolphin (ed), *The Porphyrins, Vol III, Part A, Physical Chemistry,* Academic Press, New York, (1978)

102. A.B.P. Lever, S.R. Pickens, P.C. Minor, L. Licoccia, B.S. Ramaswamy, K. Magnell, *J. Am. Chem. Soc*., **103** (1981), 6800

103. R. Taube, *Pure Appl. Chem*., **38** (1974), 427

104. A. Luoati, M.E.I. Meray, J.J. Andre, J.Simon, K.M. Kadish, M. Gross, A. Giraurdeau, *Inorg. Chem*., **24** (1985), 1175

105. J.F. Meyers, R.G.W. Canham, A.B.P. Lever, *Inorg. Chem*., **14** (1975), 461

106. A.B.P. Lever, E.R. Milaeva, G. Spier, In: A.B.P. Lever, C.C. Leznoff (eds) *Phthalocyanines: Properties and Applications*, VCH Publishers, New York, vol 3, (1993)

107. R.O. Loufty, C. Chang, *J. Chem. Phys*., **73** (1980), 2902

108. A.B.P. Lever, J.P. Wilshire, *Can. J. Chem*., **54** (1976), 2514

109. T. Nyokong, Z. Gasyna, M. Stillman, *ACS, Symp. Ser*., **321** (1986), 309

110. N.B. Mckeown, *Chem. Ind*., (1999), 92

111. P. Gregory, *High Technology Applications of Organic Colorants*, Plenum Press, New York (1991)

112. K. Morishige, S. Tomoyasu, G. Iwano, *Langmuir*, **13** (1997), 5184

113. J.E. Kuder, *J. Imaging Sci*., **32** (1988), 51

114. B. Wang, *J. Power Sources*, **152** (2005), 1

115. J-S. Zheng, X-Z. Wang, J-L. Qiao, D-J. Yang, B. Li, P. Li, H. lv, J-X. Ma, *Electrochem. Commun.* **12** (2010), 27

116. J. Zeng, S. Liao, J. Y. Lee, Z. Liang, *Int. J. Hydrogen Energy* **35** (2010), 942

117. J. J. McMahon, M. Barry, K. J. Breen, A. K. Radziwon, L. D. Brooks, M. R Blair, *J. Phys. Chem. C.* **112** (2008) 1158

118. M-H. Shao, P. Liu, R.R Adzic, *J. Am. Chem. Soc* **128** (2006), 7408

119. I. Morcos, *Electrochim. Acta* **22** (1977), 497

120. J. Zhang, K. Sasaki, E. Sutter, R.R. Adzic*, Science* **315** (2007) 220

121. F. Mirkhalaf, K. Tammeveski, D. J Schriffin, *Phys. Chem. Chem. Phys.* **11** (2009), 3463

122. M. M. Islam, T. Ohsaka, *J. Electroanal. Chem.* **623** (2008), 147

123. H. Liu, L. Zhang, J. Zhang, D. Ghosh, J. Jung, B.W. Downing, E. Whitmore, *J. Power Sources* **161** (2006), 743

124. J.S. Griffith, *Proc. R. Soc. London Ser. A*, **235** (1956) 23

125. L. Pauling, *Nature*, **203** (1964) 182

126. E. Yeager, *J. Electrochem. Soc.*, **128** (1981) 160 C

127. E. Yeager, D. Scherson, B. Simic-Glavaski, in J.D.E. McIntyre, M. Weaver, E.B. Yeager (eds.), *Chemistry and Physics of Electrocatalysis, The Electrochem. Soc. Proc. Ser.*, (1984) 247

128. H.S. Wroblowa, Y.C. Pan, G. Razumney, *J. Electroanal. Chem. Interfacial Electrochem.*, **69** (1978), 195

129. J. Zagal, M. Paez, *J Electroanal. Chem*. **339** (1992) 15

130. J. Zagal, P. Bindra, E. Yeager, *J. Electrochem. Soc*. **127** (1980) 1506

131. J. Zagal, S. Griveau, K.I Ozoemena, T. Nyokong, F. Bedioui, *J. Nanosci. Nanotechnol.* **9** (2009) 2201

132. B. Dembiska, P.J. Kulesza, *Electrochim. Acta* **54** (2009) 4687

133. A. Okunola, B. Kowalewska, M. Bron, P.J. Kulesza, W. Schuhmann, *Electrochim. Acta* **54** (2009) 4687

134. Y.W. Rhee, S. Ha, C. Rice, R.I. Masel, *J. Power Sources* **117** (2003), 35

135. R. Larsen, S. Ha, J. Zakzeski, R.I. Masel, *J. Power Sources* **157** (2006), 78

136. Z. Zhang, Y. Huang, J. Ge, C. Liu, T. Lu, W. Xing, *Electrochem. Commun* **10** (2008), 961

137. C. Rice, S. Ha, R.I. Masel, P. Waszczuk, A. Wieckowki, T. Barnard, *J. Power Sources* **111** (2002), 83

138. S. Wang, N. Kristian, S. Jiang, X. Wang, *Electrochem. Commun* **10** (2008), 961

139. J.D. Lovic, A.V. Tripkovic, S.L. Gojkovic, *J. Electroanal Chem* **581** (2005), 294

140. Z. Zhang, X. Zhou, C. Liu, W. Xing, *Electrochem Commun* **10** (2008), 131

141. R. Parson, T. VanderNoot*, J. Electroanal Chem* **257** (1988), 9

142. N. Markovic, H. Gaseiger, P. Ross, X. Jian, I. Villegas, M. Weaver, *Electrochim Acta* **40** (1995), 91

143. A. Capon, R. Parsons, *Electroanal Chem Interf Electroanal Chem* **45** (1973), 205

144. X. Xia and T.J. Iwasita, *J. Electrochem. Soc*. **140** (1993), 2559

145. M. Watanabe, Y. Futuuchi, S. Motoo, *J. Electroanal Chem* **191** (1985), 367

146. M.D. Macia, E. Herrero, J.M. Feliu, A. Aldaz, *J. Electroanal Chem* **500** (2001), 498

147. X. Zhou, C. Liu, J. Liao, T. Lu, W. Xing, *J. Power Sources* **179** (2008), 481

148. J. Javier, S. Heriban and N. Fabiola, *Regeneration of Cyanide by oxidation of thiocyanate* (1996) US Patent 5482694.

149. K. A. Singh, U. P. Singh, S. Mehtab and V. Aggarwal, *Sens. Actuators* B **125** (2007), 453

150. J. A. Cox and T. Gray, *Anal. Chem.* **60** (1988), 1710

151. M.K. Amini, S. Shahrokhian, S. Tangestaninejad, *Anal. Chim. Acta* **402** (1999) 137

152. S. Adak, A. Mazumdar, R.K. Banerjees, *J. Biol. Chem.* **272** (1997) 11049.

153. K.I. Ozoemena, T. Nyokong, *J. Electroanal. Chem*. **579** (2005) 283

154. M.J. Moorcroft, J. Davies, R.G. Compton, *Talanta* **54** (2000), 785

155. J.F. van Staden, T.A. van der Merwe, *S. Afr. J. Chem*. **51** (1998), 109

156. P. Brimblecombe, D.H. Stedman, *Nature* **298** (1982), 460

157. T. Nyokong, *Curr. Topics Electrochem*. **9** (2003), 197

158. N. Chebotareva, T. Nyokong, *J. App. Electrochem*. **27** (1997), 975

159. Z-H. Wen, T-F. Kang, *Talanta* **62** (2004), 351

160. C. Yang, Q. Lu, S. Hu, *Electroanalysis* **18** (2006) 2188

161. G. Binnig, C. Gerber, C. Quate, *Phys. Rev. Let.* **56** (1986), 930

162. S.L Flegler, J.W Heckman, K.L Klomparens, *Scanning and Transmission Electron Microscopy: An Introduction,* Oxford University Press, Cary, (1993)

163. M. De Graef, *Introduction to Conventional Transmission Electron Microscopy,* Cambridge University Press, UK, (2003)

164. M. A. O'Keefe, L. F. Allard, *Sub-Ångstrom Electron Microscopy for Sub-Ångstrom Nano-Metrology*, National Nanotechnology Initiative Workshop on Instrumentation and Metrology for Nanotechnology**,** Gaithersburg, MD (2004)

165. H.G. Brittain, *X-ray diffraction and X-ray fluorescence*, In: S. Ahuja, N. Jespersen (eds), *Comprehensive Analytical Chemistry* vol 47, Elsevier B.V, (2006)

166. R. Jenkins, R.L. Snyder, *Introduction to X-ray Powder Diffractometry,* Wiley, New York, (1996)

CHAPTER 3

Experimental

3.1 Introduction

In this chapter, a list is made of the reagent used and their grades. A detailed description is given of the synthesis of nanoMPc, MOBSPc and PtFeOCPc, as well as the process of functionalization of MWCNT. Also described are the equipment, the electrochemical measurements and non-electrochemical characterization techniques such as AFM, SEM, etc, employed in the various experimental procedures reported in this dissertation.

3.1.1. Reagents and Materials

Potassium hexacyanoferrate(II) was obtained from B. Jones Ltd., SA, potassium hexacyanoferric(III) was purchased from Bio-Zone Chemicals, SA. Potassium thiocyanate was obtained from Associated Chemicals Enterprises, SA. Hexadecyltrimethylammonium bromide (CTAB), iron(II) and cobalt(II) phthalocyanine, Pristine MWCNTs (>90% purity) were obtained from Sigma–Aldrich. Chloroform, toluene, methanol, ethanol dimethylformamide (DMF) were purchased from SAARCHEM (PTY) Ltd SA. 1,2-Dichloroethane, sodium nitrite, potassium chloride and sulphuric acid were obtained from Merck. Iron pentacarbonyl ($Fe(CO)_5$, Kanto), chloronaphthalene (Nacalai), Potassium tetrachloroplatinate (BDH). Iron(II) octa-carboxy phthalocyanine (FeOCPc), and 1,2-dibutyl-4,5-dicyanobenzene courtesy Professor Nagao Kobayashi, (Tohoku University, Sendai,

Japan). DMF was freshly distilled after drying over alumina before use. Tetrabutylammonium perchlorate (TBAP) was recrystallised from ethanol. Phosphate buffers were prepared using appropriate amounts of H_3PO_4, KH_2PO_4, K_2HPO_4 and K_3PO_4 depending on the pH and adjusted with 0.1M NaOH where needed.

3.1.2. Synthesis

3.1.2.1. *Synthesis of Nanostructured Iron(II) and Cobalt(II) Phthalocyanines*

The nanostructured iron(II) and cobalt(II) phthalocyanine complexes were prepared using the established method[1,2] as shown in Scheme 3.1. Briefly, 0.06 g iron(II) phthalocyanine or cobalt(II) phthalocyanine was dissolved in 2 mL 98% concentrated sulphuric acid, then the solution was added drop wise into 120 mL aqueous solution containing 0.18 g CTAB in an ultrasonic iced-water bath. The resulting leaf green (for iron(II) phthalocyanine) and blue (for cobalt(II) phthalocyanine) colloid solution was ultra centrifuged until separated. The obtained precipitate was washed repeatedly with water until neutral, and allowed to air-dry at room temperature for 48 h to obtain the nanostructured MPc powder.

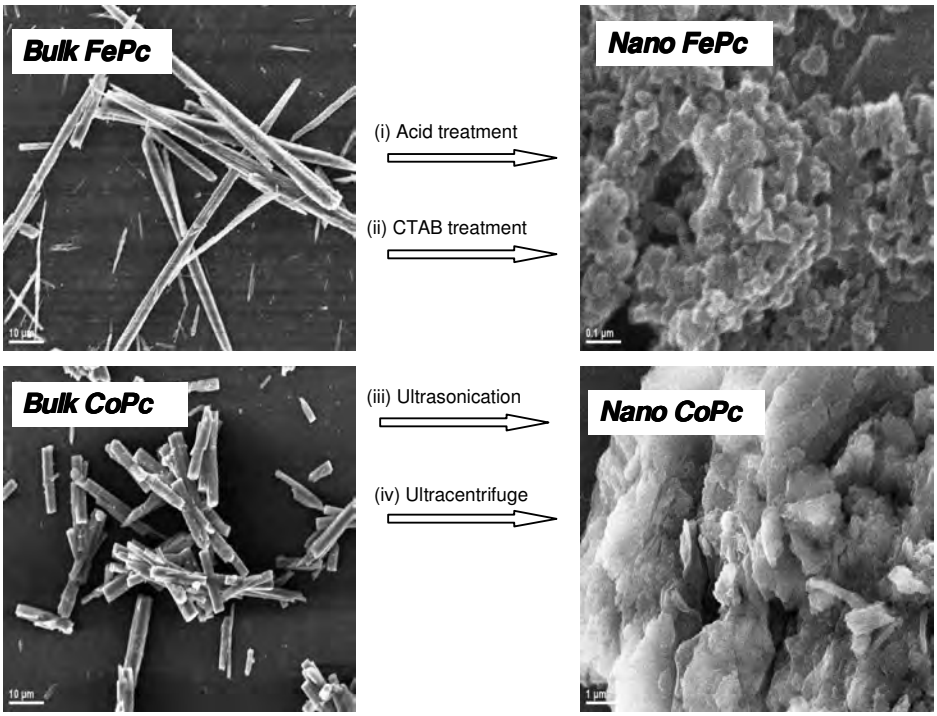

Scheme 3.1: *Schematic representation (SEM images) of the preparation of nanoMPc from the bulk MPc*

3.1.2.2. *Synthesis of Iron(II) and Cobalt(II) Octabutylsulphonylphthalocyanines*

1,2-dibutyl-4,5-dicyanobenzene (**1**) was prepared according to the method described in literature[3]. Quinoline was distilled over CaH_2 under vacuum prior to use.

Preparation of iron(II) octabutylsulphonylphthalocyanine (FeOBSPc), 2a

A mixture of (**1**) (100 mg, 0.13 mmol), and (10 μL) of iron pentacarbonyl ($Fe(CO)_5$,) was suspended in chloronaphthalene and heated at 190 °C for 2 h under argon. *(CAUTION: $Fe(CO)_5$ is suspected to be a neurotoxicant and has been ranked as one of the most*

hazardous compounds to the ecosystem and human health; so it must be used with caution). After cooling to room temperature, the reaction mixture was poured into methanol and the resultant precipitate filtered off. The filtrate was vacuum dried and the residue separated successfully, first by using short column of normal silica gel ($CHCl_3$) and finally with $CHCl_3$/MeOH (200:2 v/v) as eluent to obtain the first green-coloured fraction. Recrystallization from $CHCl_3$/methanol gave pure FeOBSPc, (**2a**). UV–visible ($CHCl_3$, λ_{max}/nm): 360, 696 MASS (ESI-FTICR) (m/z): 1551.2714, Calcd for $C_{64}H_{80}N_8S_8O_{16}FeNa$:1551.2700.

Preparation of cobalt(II) octabutylsulphonylphthalocyanine (CoOBSPc) 2b

A mixture of (**1**) (100 mg, 0.13 mmol), cobalt chloride dihydrate (23 mg, 0.14 mmol), and a catalytic amount of ammonium molybdate (120 mg) was suspended in distilled quinoline (1 mL) and heated at 190 °C for 2 h under argon. After cooling to room temperature, the reaction mixture was poured into methanol and the resultant precipitate filtered off. The filtrate was vacuum-dried and the residue separated successfully, first by using short column of normal silica gel ($CHCl_3$) and finally with $CHCl_3$/MeOH (200:2 v/v) as eluent to obtain the first blue-coloured fraction. Recrystallization from $CHCl_3$/methanol gave pure CoOBSPc, (**2b**). UV– visible ($CHCl_3$, λ_{max}/nm): 343, 678.

MASS (ESI-FTICR) (m/z): 1554.2702, Calcd for $C_{64}H_{80}N_8S_8O_{16}CoNa$: 1554.2682.

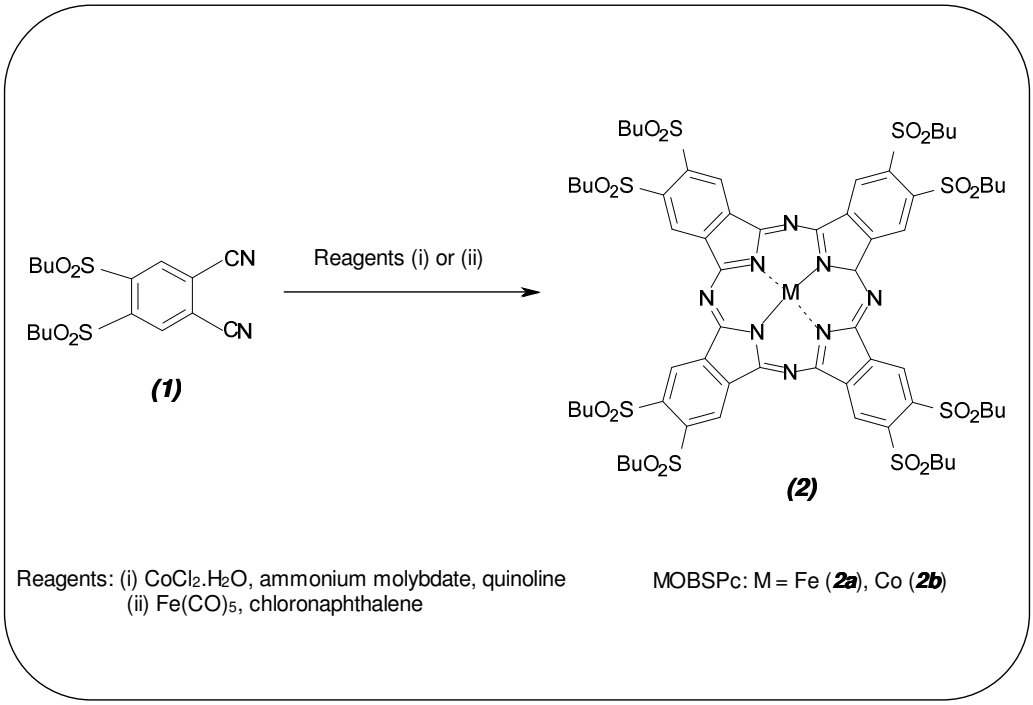

Scheme 3.2: *Synthetic route for MOBSPc*

3.1.2.3. *Synthesis of Iron(II) tetrakis(diaquaplatinum) octa-carboxyphthalocyanine ($C_{40}H_{24}N_8FeO_{24}Pt_4$)*

STEP 1

The iron(II) tetrakis(diaquaplatinum)octacarboxyphthalocyanine (PtFeOCPc) (**5**) was synthesised by adopting the same strategy reported for the cobalt derivative by Dolotova and Kaliya,[4] (Scheme 3.3). Briefly, the sodium salt of iron(II) octacarboxy phthalocyanine (**4**) (0.10 g) obtained from (**3**), was dissolved in distilled water (12 mL)

and methanol (106 mL), potassium tetrachloroplatinate (0.12g, 0.28 mmol) dissolved in 50% ethanol (190 mL) was added to the solution of (**4**), stirred for 3 h at room temperature. The resultant precipitate was filtered off after 48 h, washed with distilled water and allowed to dry (yield 0.10g, 0.24 mmol).

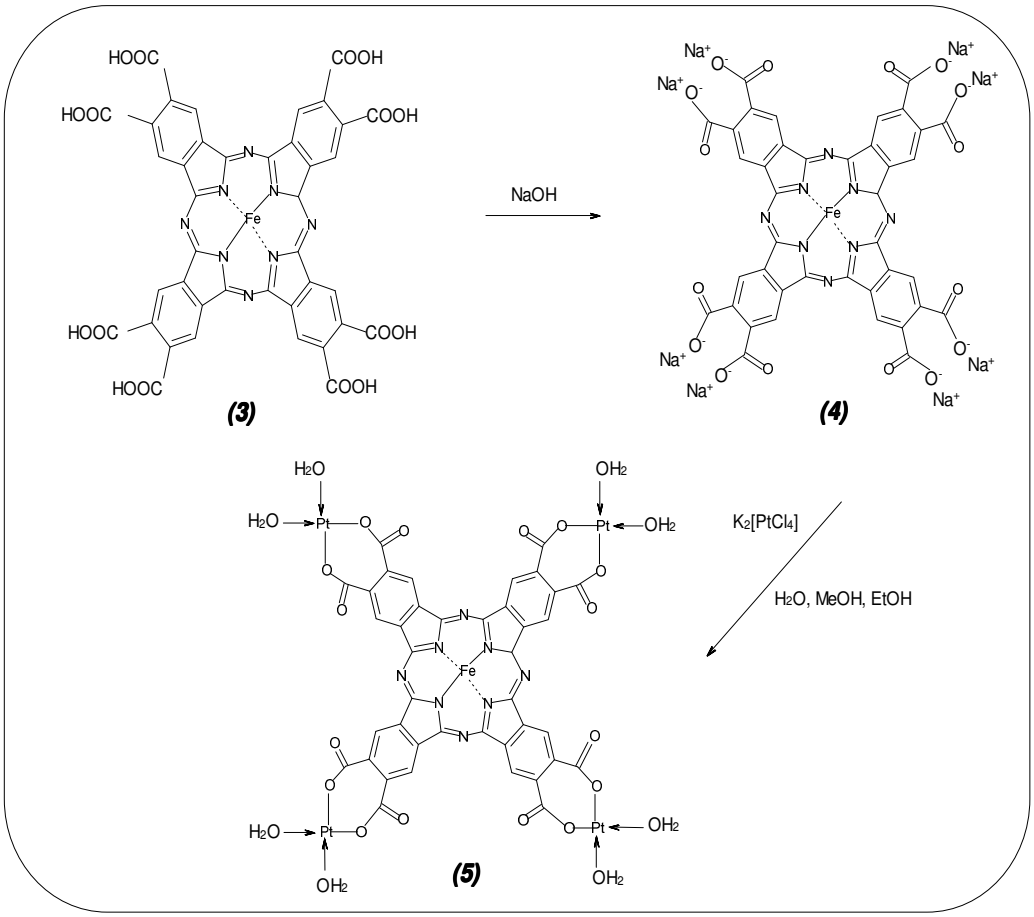

***Scheme 3.3**: Synthetic route for PtFeOCPc*

STEP 2

Potassium tetrachloroplatinate (0.10g, 0.24 mmol) dissolved in 50% ethanol (119 mL) was added to the suspension of the product obtained in step 1 which has already been dissolved in a mixture of distilled water (20 mL) with methanol (85 mL), stirred for 3 h at room temperature. The resultant precipitate was filtered off after 48 h, washed with distilled water, ethanol, acetone, and ether and allowed to dry (yield 0.070g). The dried product (**5**) is a dark green-coloured crystalline compound. (UV-visible (DMF, λ_{max}/nm): 313, 450, 685. FTIR ν_{max}/cm^{-1}: 3400(ν_{O-H}), 1605(ν_{C-O}), 1550(ν_{C-O}), 1200(ν_{COO^-}). Elemental analysis: Found C, 25.60; H, 1.39; N, 6.34. $C_{40}H_{24}N_8FeO_{24}Pt_4$ requires C, 26.14; H, 1.31; N, 6.10)

3.1.3. *Purification of Multi-Walled Carbon Nanotubes*

Pristine MWCNTs (> 90% purity) were purified and acid-functionalised as described before.[5] Briefly, 1 g of MWCNTs was added to 140 mL of 2.6 M HNO_3, and the mixture was refluxed for 48 h. The multi-walled carbon nanotubes sediment was separated by centrifugation, and washed with distilled water. It was then sonicated in a concentrated mixture of H_2SO_4 and HNO_3 (3:1 ratio) at 40 °C for 24 h. The sediment was thereafter washed with distilled water, stirred for 30 minutes in a 4:1 H_2SO_4/H_2O_2 mixture at 70 °C, and washed with

distilled water. The final purified and functionalised MWCNT slurry was then oven-dried at 50 ^{o}C for 48 h.

3.1.4. *Electrode Modification Procedure*

The working electrode used for electrochemical studies in this thesis is bare edge plane pyrolytic graphite electrode herein referred to as EPPGE, fabricated in-house from EPPG plate (Le Carbone, Sussex, UK). Electrical contact with the disk was maintained through an inserted copper wire held in place with conducting silver varnish. The working electrode for the rotating disk electrode experiment was fabricated in-house from an EPPG plate housed in an AUTOLAB–RDE Teflon cover. Prior to modification, the bare EPPGE was first polished with slurries of aluminium oxide nanopowder, mirror finished on a Buehler felt pad and then subjected to ultrasonic stirring in acetone and ultrapure water respectively for 3 min to remove residual alumina particles that might be trapped at the surface. 1 mg MWCNT was dispersed in 1mL DMF with the aid of ultrasonic stirring. 15 µL of the MWCNT solution was cast on the EPPGE surface and allowed to dry at room temperature to prepare the EPPGE-MWCNT electrode. 15 µL of the MPc complexes prepared in the same manner was cast onto the surface of the bare EPPGE to prepare the EPPGE-MPc electrode or cast onto the surface of the EPPGE-MWCNT to prepare the EPPGE-MWCNT-MPc electrode.

3.1.5. *Electrochemical Procedure and Instrumentation*

All electrochemical studies were performed with Autolab potentiostat PGSTAT 20, driven by the General Purpose Electrochemical Systems data processing software (GPES 4.9) (Eco-Chemie, Utrecht, The Netherlands), equipped with a conventional three-electrode system (Figure 3.1), were the working electrode is either a bare EPPGE (d = 3.0 mm) or modified EPPGE. An Ag|AgCl (saturated 3 M KCl) was used as reference electrode and a platinum rod as a counter electrode. Solution electrochemistry was performed in ~1mM of MPc complexes in dry DMF containing 0.1 M tetrabutylammonium perchlorate (TBAP) as the supporting electrolyte under nitrogen atmosphere. Glassy carbon electrode (0.07 cm^2), platinum rod and Ag|AgCl wire were used as the working, counter and reference electrodes, respectively.

Electrochemical impedance spectroscopy (EIS) measurements were performed with Autolab Frequency Response Analyser (FRA) software between 10 kHz and 10 mHz using a 5 mV rms sinusoidal modulation in 0.1M of $K_4Fe(CN)_6$ and 0.1M $K_3Fe(CN)_6$ (1:1) mixture containing 1.0 M KCl at the $E_{1/2}$ of the $[Fe(CN)_6]^{3-/4-}$ (0.30 V vs. Ag|AgCl saturated KCl). Solutions were deoxygenated by a stream of high purity nitrogen for at least 5 min before running the experiment and the solution was protected from air by a blanket of nitrogen during the experiment.

Oxygen reduction was studied using cyclic voltammetry. The rotating disk electrode (RDE) technique was also used in order to eliminate mass transport problems, employing an AUTOLAB–RDE (Eco-Chemie, Utrecht, The Netherlands), For the RDE, 30 mL of 0.1 M NaOH solution was used as the electrolyte to study the reduction of oxygen after bubbling with high purity nitrogen (99.99%) and oxygen, as the case may be, for 15 minute. The voltammograms were recorded using linear sweep potential scan between 0.40 to -0.80 V.

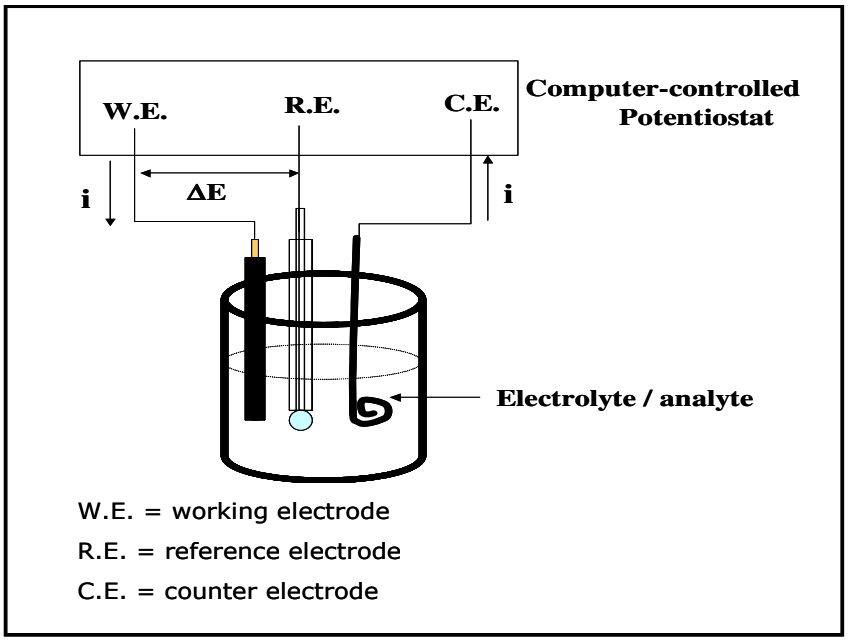

Figure 3.1: *Diagrammatic presentation of a conventional three-electrode system*

A BENCHTOP, 420A (LABOTEC) pH meter was used for pH measurements. Ultra pure water of resistivity 18.2 MΩ.cm was obtained from a Milli-Q Water System (Millipore Corporation, Bedford,

MA, USA) and was used throughout for the preparation of solutions. Ultrasonic bath (INTEGRAL SYSTEMS) was used for ultrasonic stirring.

All the AFM experiments were performed with AFM 5100 System (Agilent Technologies, USA) using a contact mode AFM scanner interfaced with a PicoView 1.4.3 controller (scan range 1.25 μm in *x*–*y* and 2.322 μm in *z*). Silicon type PPP-CONT-20 (Nanosensors®) of thickness 2.0±1.0 μm, length 450±10 μm, width 50±7.5 μm, spring constants 0.02–0.77 Nm^{-1}, resonant frequencies of 6–21 kHz and tip height of 10–15 μm were used. All images were taken in air at room temperature in an anti-vibration chamber at scan rates 0.5 – 0.6 lines s^{-1}. Field emission scanning electron microscopy (FESEM) images were captured with JEOL JSM 5800 LV (Japan). Morphological analyses of the different MPc complexes were carried out and viewed at an accelerating voltage of 5 k*e*V and using the lowest beam current in order to avoid sample damage. Transmission electron microscopy (TEM), imaging and energy-dispersive X-ray spectroscopy (EDS) analysis were carried out using JEOL JEM– 2100 F/HT TEM, operating at an accelerating voltage of 200 KeV equipped with EDS. Digital processing of the TEM images was carried out using UTHSCSA ImageTool® software version 3.0. The UV – Visible spectra were measured using a Cary 300 UV- Visible Spectrophotometer, driven by Varian software version 3.0 at a scan rate of 600 nm/min. IR spectra were measured using a Perkin Elmer Spectrum RX 1 FT – IR system attached with a MIRacle ATR with diamond / ZnSe crystal plate for

transmission in the 400 – 4000 cm^{-1} range. Elemental analysis was carried out with a Carlo Erba NA 1500 Nitrogen Carbon Sulphur Analyser. Gas Chromatography (GC) was used to separate the gases, i.e. N (in the form of N_2), C (in the form of CO_2) and S (in the form of SO_2), using a He carrier gas and a thermal conductivity detector, driven by PeakNet software (Dionex Corporation, May 1998), with an external A/D interface (UI20 Universal Interface, Dionex). XRD analysis was carried out using a back loading preparation method. It was analyzed with a PANalytical X'Pert Pro powder diffractometer with X'Celerator detector and variable divergence and receiving slits with Fe filtered Co-Kα radiation. The diffraction patterns were collected from 10° to 110°. The phases were identified using X'Pert Highscore plus software.

References

1. M. Siswana, K.I. Ozoemena, T. Nyokong, *Talanta* **69** (2006) 1136.
2. Y.Wang, K. Deng, L. Gui, Y. Tang, J. Zhou, L. Cai, J. Qui, D. Ren, Yq.Wang, *J. Colloid Interf. Sci*. **213** (1999) 270
3. K.M. Keshavarz, B. Knight, G. Srdanov, F. Wudl, *J. Am. Chem. Soc*. **117** (1995) 11371
4. O.V. Dolotova, O.L. Kaliya, *Russ. J. Coord. Chem.* **33** (2007), 111
5. J. Liu, A.G. Rinzler, H. Dai, J.H. Hafner, R. Kelley Bradley, P.J. Boal, A. Lu, R.E. Smalley, *Science* **280** (1998), 1253